Nature Communications

https://doi.org/10.1038/s41467-026-69996-8

Article in Press

DNA-PK-mediated phosphorylation of STAT6 establishes a non-canonical type 2 immunity axis to prevent macrophage senescence

Received: 7 August 2025

Accepted: 12 February 2026

Cite this article as: Zhou, Z., Li, X., Wang, Y. *et al.* DNA-PK-mediated phosphorylation of STAT6 establishes a non-canonical type 2 immunity axis to prevent macrophage senescence. *Nat Commun* (2026). https://doi.org/10.1038/s41467-026-69996-8

Zhao Zhou, Xinmeng Li, Yushuang Wang, Long Liang, Chunyang Wang, Yongchang Sun, Dongmei Wu & Yifu Qiu

DNA-PK-mediated phosphorylation of STAT6 establishes a non-canonical type 2 immunity axis to prevent macrophage senescence

Zhao Zhou[1], Xinmeng Li[1], Yushuang Wang[1], Long Liang[2], Chunyang Wang[1], Yongchang Sun[2*], Dongmei Wu[1,3*], Yifu Qiu[1,3,4*]

[1]State Key Laboratory of Membrane Biology, Beijing Key Laboratory of Cardiometabolic Molecular Medicine, Institute of Molecular Medicine, College of Future Technology, Peking University, Beijing 100871, China.

[2]Department of Respiratory and Critical Care Medicine, Peking University Third Hospital and Research Center for Chronic Airway Diseases, Peking University Health Science Center, Beijing, China

[3]Peking-Tsinghua Center for Life Sciences, Academy for Advanced Interdisciplinary Studies, Peking University, Beijing 100871, China.

[4]Frontiers Medical Center, Tianfu Jincheng Laboratory, Chengdu, China

*Correspondence: suny@bjmu.edu.cn, dongmei.wu@pku.edu.cn, yifu.qiu@pku.edu.cn

Abstract

Macrophage senescence drives inflammaging, a chronic, age-related inflammation. To date, the protective mechanisms against inflammaging are poorly defined. Here, we identify DNA-PK-mediated phosphorylation of murine STAT6 at serine 807 (Ser807) as a crucial post-translational modification for preventing macrophage senescence. Ser807 phosphorylation blocks STAT6 ubiquitination-mediated degradation and promotes STAT6 partnering with PU.1 to activate DNA repair genes. Macrophages lacking Ser807 phosphorylation exhibit DNA repair defects, undergo senescence, and fuel inflammaging. In vivo, the phosphor-null STAT6 mutant (STAT6(S807A)) accelerates macrophage senescence, tissue fibrosis, and systemic aging. Adoptive transfer of phosphomimetic STAT6(S807E)-expressing macrophages rescues accelerated aging. Importantly, phosphorylation of human STAT6 at the homologous residue (Ser817) is significantly reduced in the lungs of patients with chronic obstructive pulmonary disease (COPD), correlating with increased DNA damage and senescence. Thus, our findings reveal a DNA-PK-STAT6 axis enacting a non-canonical type 2 immunity via DNA repair to prevent macrophage senescence, presenting a therapeutic target for healthy aging.

Introduction

The immune system serves as a critical gatekeeper of organismal health, detecting and counteracting diverse stresses, including infection and endogenous perturbations[1, 2]. However, aging drives deterioration of immune surveillance, fostering chronic inflammation ("inflammaging") that accelerates aging and age-related pathologies[3, 4, 5, 6, 7, 8]. Central to this process are senescent immune cells, which secrete pro-inflammatory cytokines and matrix-remodeling factors—collectively termed the senescence-associated secretory phenotype (SASP)—thereby disrupting tissue homeostasis[9, 10]. Critically, as one of the most potent immune cells, macrophages serve as a primary inflammatory mediator in numerous contexts, particularly in aging. Notably, inflammatory macrophages are implicated in a wide range of age-related diseases and are key drivers of inflammaging. This central role positions macrophage dysfunction at the nexus of age-related functional decline[11, 12, 13, 14].

Macrophage functional diversity arises from integration of extracellular signals, including cytokines, pathogens and tissue environment[15, 16]. Canonical type 2 immunity, driven by IL-4/IL-13 and STAT6-dependent alternative activation, exemplifies this plasticity[17]. Beyond its established role, STAT6 also counteracts inflammation-related transcription[18, 19] and mediates STING-TBK1-triggered antiviral responses[20]. Notably, we recently identified a pivotal role for STAT6 in mitigating aging through the regulation of DNA repair genes, such as *Brca1* and *Ube2t*[13]. While STAT6 functions are stimulus-dependent, the signals driving its non-canonical, senescence-protective activation remain undefined.

Persistent DNA damage and dysregulated DNA damage response (DDR) pathways are hallmarks of aging and senescence[3, 21]. DDR kinases—DNA-dependent protein kinase (DNA-PK), ataxia-telangiectasia mutated (ATM) and ATM- and Rad3-related (ATR)—orchestrate distinct DNA repair

programs[22]. Intriguingly, DNA-PK also senses self- and viral DNA, bridging DDR to immune and inflammatory responses[23, 24, 25]. Despite these links, whether DNA damage and DDR contribute to STAT6 non-canonical functions is unknown.

In this study, we identify a DNA-PK-dependent phosphorylation of STAT6 that establishes a non-canonical, senescence-protective function in macrophages. This modification stabilizes STAT6, enabling a transcriptional partnership with PU.1 to enhance DNA repair and prevent inflammaging. Importantly, this phosphorylation is significantly reduced in lungs from chronic obstructive pulmonary disease (COPD) patients, correlating with heightened DNA damage and senescence markers. Our findings reveal a direct molecular link between DNA damage sensing and immune cell senescence, presenting a target for interventions against inflammaging and age-related diseases.

Results

DNA damage enhances STAT6 activation via DNA-PK

To explore non-canonical roles for STAT6 in macrophage senescence, we first assessed whether DDR activation coincided with STAT6 signaling. Treatment with the DNA-damaging chemotherapy agent etoposide (Eto) and IL-4 synergistically enhanced phosphorylation of Tyr641—a residue essential for STAT6 dimerization and canonical activation—in murine thioglycolate-elicited peritoneal macrophages (Thio-PM) (Fig. 1A, B and Supplementary Fig. 1A). Similarly, irradiation or oxidative stress potentiated STAT6 activation (Supplementary Fig. 1B, C), and luciferase reporter assays confirmed elevated STAT6 transcriptional activity in HEK 293T cells (Supplementary Fig. 1D).

We next investigated the mechanism underlying DNA damage-induced STAT6 activation. As DNA damage did not engage JAK1 (Supplementary Fig. 1E), the canonical upstream kinase[26], we next explored whether DNA damage activates via the cGAS-STING pathway[27]. While the STING-TBK1 axis was reported to promote Tyr641 phosphorylation of STAT6 in an antiviral immune response[20], genetic ablation or pharmacological inhibition of STING failed to abrogate STAT6 activation by DNA damage (Supplementary Fig. 1F, G). We therefore focused on DDR kinases (ATM, ATR, DNA-PK, and their effector CHKs)[22]. Inhibition of DNA-PK with NU7026 attenuated DNA damage-induced STAT6 phosphorylation and impaired DNA repair in Thio-PMs. In contrast, inhibitors targeting other kinases, such as KU55933 (ATM), Berzosertib (ATR), and AZD7762 (CHK1/2), showed no significant effect (Fig. 1C and Supplementary Fig. 1H). CRISPR/Cas9-mediated knockout of *Prkdc* (encoding DNA-PK) prevented STAT6 activation, whereas loss of other DDR kinases had no effect (Fig. 1D). DNA-PK inhibition also suppressed STAT6 transcriptional activity in RAW 264.7 cells (Fig. 1E). Analogous results were observed in primary mouse embryonic fibroblasts (MEF) (Supplementary Fig. 1I). These data collectively demonstrate that DNA damage enhances STAT6 activation in a DNA-PK-dependent manner.

DNA-PK directly phosphorylates murine STAT6 at Ser807

Given the specific requirement for DNA-PK (but not downstream CHKs) in DNA damage-induced STAT6 Tyr641 phosphorylation (Fig. 1D) and the known activation of DNA-PK kinase activity by DNA damage[28], we hypothesized that DNA-PK directly phosphorylates STAT6. TurboID-based proximity labeling confirmed a DNA damage-dependent interaction between DNA-PK and STAT6 in RAW 264.7 cells, which was absent for ATM or ATR (Fig. 2A). This interaction was further validated in situ by proximity ligation assay upon etoposide treatment in Thio-PMs (Fig. 2B, C and Supplementary Fig. 2A).

Mass spectrometry identified STAT6 residues phosphorylated by DNA-PK, four of which were also predicted by GPS5.0[29] (Supplementary Fig. 2B and Supplementary Data 1, 2). Three of the four residues are evolutionarily conserved across species (Fig. 2D and Supplementary Fig. 2C). Among them, only mutations at Ser807 (phospho-null S807A or phosphomimetic S807E) altered STAT6 Tyr641 phosphorylation in RAW 264.7 cells (Fig. 2E and Supplementary Fig. 2D). Crucially, the STAT6(S807E) mutant rescued DNA damage-induced STAT6 activation in DNA-PK-deficient Thio-PMs (Fig. 2F) and enhanced STAT6 transcriptional activity in RAW 264.7 cells (Fig. 2G), indicating that Ser807 phosphorylation is functionally critical.

To directly monitor Ser807 phosphorylation, we generated a phospho-specific antibody (Supplementary Fig. 2E). As expected, DNA-PK inhibition or genetic loss (*Prkdc*, *Ku70,* or *Ku80*) abolished Ser807 phosphorylation in Thio-PMs (Fig. 2H–J, and Supplementary Fig. 2F). Notably, this modification was independent of canonical STAT6 signaling, as IL-4–induced Tyr641 phosphorylation (or its inhibition) under Eto treatment did not affect Ser807 phosphorylation (Fig. 2K). Moreover, DNA damage robustly induced Ser807 phosphorylation even in a STAT6 Y641F mutant (Fig. 2L), confirming its independence from Tyr641 modification. Consistent with STAT6–DNA-PK interactions occurring primarily in the cytoplasm (Fig. 2B and Supplementary Fig. 2G), pharmacological inhibition of EPAC (mediating DNA-PK nuclear export[30]) reduced Ser807 phosphorylation (Supplementary Fig. 2H, I). Collectively, these data establish that DNA-PK directly phosphorylates STAT6 at Ser807 to drive its activation in response to DNA damage.

Phosphorylation at Ser807 stabilizes STAT6 by impeding ubiquitin-mediated degradation

Since STAT6 activation is modulated by both kinase signaling and negative regulators (e.g., dephosphorylation, degradation; see Fig. 3A), we investigated how Ser807 phosphorylation enhances Tyr641 phosphorylation. Ser807 phosphorylation did not alter STAT6's association with JAK1 or IL-4Rα, nor did DNA damage regulate JAK1 activity (Supplementary Fig. 1E, 3A), excluding upstream kinase involvement. Strikingly, the phosphomimetic STAT6(S807E) mutant exhibited prolonged Tyr641 phosphorylation after extended IL-4 stimulation (4h vs. 30 min; Fig. 3B, C) and an extended half-life (Fig. 3D, E), indicating Ser807 phosphorylation stabilizes STAT6.

Mechanistically, Ser807 phosphorylation reduced proteasomal (but not lysosomal) degradation of STAT6 (Fig. 3F and Supplementary Fig. 3B). DNA damage diminished K48-linked ubiquitination of STAT6 in a DNA-PK–dependent manner (Fig. 3G), and the S807E mutant displayed reduced ubiquitination versus wild-type (WT) STAT6 (Supplementary Fig. 3C). Relative to WT STAT6, S807E impaired STAT6's interaction with RING finger protein 128 (RNF128), an E3-ligase for Tyr641-phosphorylated STAT6[31] (Fig. 3H–J). However, Ser807 phosphorylation did not affect STAT6's interaction with Cbl proto-oncogene B (CBL-B), another STAT6-associated E3-ligase[32], whose expression was less than RNF128 in macrophages (Supplementary Fig. 3D, E). When combining prediction by GPS-Uber and analysis of qPTM database[33, 34], we identified six potential RNF128-catalyzed ubiquitination residues including Lys228, Lys319, Lys366, Lys450, Lys595 and Lys636 (Supplementary Fig. 3F). Of those, we used mutagenesis assays to identify that RNF128 ubiquitinated STAT6 at Lys319 and Lys595 (Fig. 3K and Supplementary Fig. 3G). Lys450 of STAT6 was ubiquitinated by TRAF3[35], which did not affect STAT6 stabilization after IL-4 stimulation (Supplementary Fig. 3H). We next determined that the K319R, but not the K595R mutant, was resistant to RNF128-mediated

STAT6 degradation (Fig. 3L). Consistently, the K319R mutant rescued the instability of the non-phosphorylatable S807A mutant (Fig. 3M). These data indicate that Ser807 phosphorylation of STAT6 inhibits its interaction with RNF128, thereby suppressing RNF128-catalyzed K319 ubiquitination and proteasomal degradation.

In parallel, we assessed phosphatases (SHP1, PTPN1, PTPN2) reported to dephosphorylate STAT6-Tyr641 and inactivate it[36, 37, 38]. S807E reduced STAT6's interaction with PTPN1 but not SHP1/PTPN2 (Fig. 3N, O, and Supplementary Fig. 3I, J). However, PTPN1 inhibition only modestly enhanced Tyr641 phosphorylation in S807E (Fig. 3P). Collectively, these data demonstrate that Ser807 phosphorylation primarily enhances STAT6 activation by counteracting RNF128-dependent ubiquitin-proteasome degradation.

Ser807 phosphorylation of STAT6 orchestrates DNA repair in macrophages via PU.1 synergy

Given STAT6's established role in DNA repair[13] and our discovery that DNA-PK phosphorylates STAT6 at Ser807 during DNA damage, we hypothesized that Ser807 phosphorylation regulates DNA repair. To test potential roles of Ser807-phosphorylation-mediated STAT6 activation *in vivo*, we generated *Stat6*^{S807A} and *Stat6*^{S807E} knock-in mice by CRISPR/Cas9 technology (Supplementary Fig. 3N–P). Above all, molecular activities of phosphomimetic S807E were consistent in primary macrophages from these knock-in mice (Supplementary Fig. 3Q, R). Next, RNA-seq of Thio-PMs revealed distinct transcriptomes across *Stat6*$^{WT/WT}$, *Stat6*$^{S807A/S807A}$ and *Stat6*$^{S807E/S807E}$ genotypes (Fig. 4A and Supplementary Fig. 4A). Gene Set Enrichment Analysis (GSEA) showed enhanced "DNA Repair" gene signatures in *Stat6*$^{S807E/S807E}$ macrophages, while inflammatory and senescence pathways dominated in *Stat6*$^{S807A/S807A}$ cells (Fig. 4B). Both homologous recombination (HR) and nonhomologous end joining

(NHEJ) repair pathways were potentiated in *Stat6*$^{S807E/S807E}$ macrophages, confirmed by DNA repair reporter assays (Supplementary Fig. 4A–D). Consistently, *Stat6*$^{S807E/-}$ macrophages exhibited accelerated DNA repair and reduced γH2AX foci—effects abrogated by blocking Tyr641 phosphorylation (Fig. 4C, D and Supplementary Fig. 4E–G). Mechanistically, Ser807 phosphorylation enabled STAT6 to bind to the loci of DNA repair genes (such as *Brca1* and *Ube2t*) and transactivate them (Fig. 4E and Supplementary Fig. 4H).

Although Ser807 phosphorylation occurred in MEFs, *Brca1*/*Ube2t* induction was minimal (Supplementary Fig. 4I), suggesting macrophage-specific cofactors. Integrating transcriptomics with transcription factor (TF) prediction of *Brca1* and *Ube2t* by AnimalTFDB[39], we identified three TFs may serve as cofactors: PU.1, TAL1 and SPI-C (Fig. 4F). Among these, PU.1 emerged as a key focus due to its established role as a master regulator of macrophage homeostasis[40]. Reanalysis of a public single-cell sequencing dataset[41] revealed that *Spi1* (encoding PU.1) was uniquely highly expressed in macrophages (with minimal *Spi1* expression detected in some B cells), but not in other cell types (Supplementary Fig. 4J, K). Co-IP and proximity assays revealed direct STAT6-PU.1 binding, strengthened by Ser807 phosphorylation (Fig. 4G, H and Supplementary Fig. 4L). PU.1 recruitment to *Brca1*/*Ube2t* loci was enhanced by phosphomimetic STAT6 and diminished by non-phosphorylatable STAT6 (Fig. 4I and Supplementary Fig. 4M). Critically, PU.1 inhibition abolished STAT6-driven DNA repair gene expression and functional repair, while its expression enhanced their transcription (Fig. 4J, K and Supplementary Fig. 4N). Strikingly, ectopic PU.1 expression enabled the phosphomimetic STAT6(S807E) mutant to induce transcription of DNA repair genes in MEFs (Supplementary Fig. 4O). These data indicate that Ser807-phosphorylated STAT6 cooperates with PU.1 to drive macrophage-specific DNA repair programs.

In addition, higher *Chil3* expression in *Stat6*$^{S807E/S807E}$ Thio-PMs might indicate its STAT6-mediated polarization (Supplementary Fig. 4A). From experimental results, we found no changes during M1-polarization among them (Supplementary Fig. 5A). Although some M2-polarization associated genes were upregulated in *Stat6*$^{S807E/S807E}$ Thio-PMs, efficient polarization was induced in *Stat6*$^{S807A/S807A}$ Thio-PMs, similar to wild-type (Supplementary Fig. 5B), suggesting minimal effect of Ser807 phosphorylation on macrophage polarization.

Ser807 phosphorylation of STAT6 suppresses macrophage senescence and preserves immunosurveillance

Given the established link between DNA repair and senescence resistance[21], we hypothesized that Ser807 phosphorylation protects macrophages from senescence. Indeed, macrophages from *Stat6*$^{S807A/-}$ knock-in mice exhibited profound senescence hallmarks upon DNA damage, including elevated expression of senescence markers and SASP factors as well as anti-apoptosis genes, decreased LaminB1 protein, abundant ROS, reduced proliferative capacity (fewer Ki-67/EdU^{+} cells), increased SA-β-Gal activity and lipofuscin accumulation (Fig. 5A–G, and Supplementary Fig. 5C–G). To isolate cell-intrinsic effects, we co-transferred equal numbers of *Stat6*$^{WT/WT}$, *Stat6*$^{S807A/S807A}$, and *Stat6*$^{S807E/S807E}$ resident peritoneal macrophages (Res-PM) into recipient mice (Fig. 5H). After 14 days, *Stat6*$^{S807A/S807A}$ Res-PMs were significantly decreased, confirming their senescence susceptibility *in vivo* (Fig. 5I and Supplementary Fig. 5H). We next assessed functional consequences. *Stat6*$^{S807A/S807A}$ Thio-PMs showed impaired phagocytosis *in vitro* (Supplementary Fig. 5I–L) and defective clearance of both bacteria and senescent cells *in vivo* (Fig. 5J, K). Collectively, these data demonstrate that Ser807 phosphorylation preserves macrophage homeostasis by preventing senescence and maintaining immunosurveillance competence.

Loss of Ser807 phosphorylation induces tissue senescence and impairs mouse healthspan

Based on the established links between DNA damage, inflammation, and aging[3], we investigated the role of STAT6 Ser807 phosphorylation in organismal aging. Compared with *Stat6*$^{S807E/S807E}$ mice, *Stat6*$^{S807A/S807A}$ ones exhibited profound aging phenotypes including impaired motor coordination (rotarod, hanging tests), reduced endurance (treadmill), cognitive decline (Y-maze working memory), and decreased bone density (Fig. 6A–E). On molecular level, loss of Ser807 phosphorylation was associated with robust expression of senescence markers and SASP in epididymal white adipose tissue (eWAT), liver and lung from *Stat6*$^{S807A/S807A}$ mice (Fig. 6F, G and Supplementary Fig. 6A), and enhanced SA-β Gal activity was present in eWAT (Fig. 6H), indicating that loss of Ser807 phosphorylation accelerates aging. Through cell separation, macrophages (F4/80+ cells) were found as major senescence contributor in these tissues (Supplementary Fig. 6B–F). Besides, we also found similar aging phenotypes in female mice (Supplementary Fig. 6G–L).

To assess therapeutic potential, we transferred bone-marrow derived macrophages (BMDM) into accelerated-aging *Stat6*$^{f/f}$;*Lyz2*^{Cre} mice[13] (Supplementary Fig. 7B). We first determined the optimal number of BMDMs for transfer. In preliminary experiments, transferring 2×10^6 cells effectively reduced senescence in eWAT (Supplementary Fig. 7C). Only *Stat6*$^{WT/-}$ or *Stat6*$^{S807E/-}$ macrophages rescued motor function and reduced tissue senescence (Supplementary Fig. 7D–G). Furthermore, we used naturally aged mice to validate the efficacy of macrophage transfer (Fig. 6I). Critically, in naturally aged mice, transfer of *Stat6*$^{S807E/S807E}$ BMDMs improved healthspan metrics: body weight, motor function, working memory, and physical performance (Fig. 6J–N, and Supplementary Fig. 7H). On molecular level, transfer of these macrophages effectively attenuated age-related organ senescence, as demonstrated by significant reductions in key senescence markers, including SASP factors and SA-β-Gal activity across organs (Fig.

6O–Q, and Supplementary Fig. 7I, J). These data establish adoptive transfer of Ser807-phosphorylated STAT6 macrophages as a potent strategy to counteract aging-associated decline.

Ser807 phosphorylation of STAT6 confers protection against senescence-driven pulmonary fibrosis

Based on the critical role of alveolar macrophages (AM) in lung homeostasis and their susceptibility to DNA damage-induced dysfunction[42], we assessed the pathophysiological relevance of STAT6 Ser807 phosphorylation. Initially, Ser807 phosphorylation conservatively regulate STAT6 activation and transcription of DNA repair genes in AMs (Fig. 7A and Supplementary Fig. 3Q). Following bleomycin challenge (a DNA-damaging agent), AMs from *Stat6*$^{S807A/S807A}$ mice exhibited exacerbated senescence markers (Fig. 7B–D). Conversely, *Stat6*$^{S807E/S807E}$ mice displayed significantly attenuated pulmonary fibrosis, and improved survival (Fig. 7E–G). Through immunoblot analysis, we documented that cellular senescence, collagen deposition and SMAD2/3 activation were greatly reduced in *Stat6*$^{S807E/S807E}$ compared with *Stat6*$^{S807A/S807A}$ mice (Fig. 7H). Importantly, adoptive transfer of *Stat6*$^{S807E/S807E}$ AMs into bleomycin-treated mice mitigated fibrosis, as evidenced by suppressed fibrotic marker expression, restored alveolar architecture, and improved histological scores. Conversely, transfer of *Stat6*$^{S807A/S807A}$ AMs exacerbated pathology (Fig. 7I-L). These data indicate that STAT6 Ser807 phosphorylation preserves AM function to protect against senescence-driven lung fibrosis.

Ser817 phosphorylation of STAT6 is reduced in the lungs of COPD patients

Based on proteogenomic identification of human STAT6 phosphorylation at Ser817[43] (homologous to murine Ser807; shown in Supplementary Fig. 2C), we investigated its functional conservation. We first validated the phospho-specific antibody against human pSTAT6-Ser817 (Supplementary Fig. 8A). We next demonstrated that DNA-PK directly phosphorylated STAT6-Ser817 upon DNA damage in THP-1-

differentiated macrophages, as well as the primary human monocyte-derived macrophages (hMDM) (Fig. 8A and Supplementary Fig. 8B). Importantly, phosphomimetic STAT6(S817E) enhanced IL-4-induced Tyr641 phosphorylation (Supplementary Fig. 8C). Functionally, Ser817 phosphorylation promoted DNA repair, suppressed senescence, and enhanced phagocytosis in human macrophages (Fig. 8C–F and Supplementary Fig. 8D), confirming its evolutionary conservation.

Analysis of human tissues (GTEx) revealed positive correlations between *PRKDC* (DNA-PK) and DNA repair genes (*UBE2T*, *BRCA1*) in lung and adipose tissue[44] (Supplementary Fig. 8E). As a leading cause of death and disability, COPD is highly associated with aging and environmental stress[8, 45]. In COPD, we observed an accumulation of senescent macrophages in patient lungs (Fig. 8G–I), a marked reduction of STAT6-Ser817 phosphorylation (Fig. 8J, K), and strong negative correlations between pSer817 levels and DNA damage/senescence (Fig. 8L, M). These findings nominate STAT6-Ser817 hypophosphorylation as a biomarker and therapeutic target in COPD pathogenesis.

Discussion

Macrophages are pivotal regulators of tissue homeostasis, and their senescence drives age-related pathologies[6, 7, 11, 13, 46, 47]. However, the molecular pathways governing macrophage senescence remain poorly defined. Here, we identify the DNA-PK–STAT6–PU.1 axis as a critical guardian against macrophage senescence, revealing how DNA damage reprograms STAT6 into a DNA repair effector (Supplementary Fig. 8F). We demonstrate that DNA-PK–mediated phosphorylation of STAT6 at Ser807 (Ser817 in humans) creates a molecular rheostat: it stabilizes STAT6 by blocking RNF128-dependent

ubiquitination, licenses PU.1-coordinated transcription of DNA repair genes (*Bcra1*, *Ube2t*), and ultimately confers a non-canonical type 2 immunity to shield macrophages from senescence. This pathway's conservation in humans—and its disruption in COPD—highlights STAT6 phosphorylation as a druggable nexus linking genomic stress to immune resilience.

While mitochondrial dysfunction and microbiota are reported as important factors in T and B cell senescence, DNA damage plays a central role in cellular senescence[21,48, 49, 50]. Yet, how immune cells—particularly macrophages—orchestrate resistance remained unclear. Our work positions STAT6 as a molecular integrator of DDR and immune signaling: DNA-PK-mediated Ser807 phosphorylation converts STAT6 from a canonical cytokine transducer[17] into a DNA repair effector. This non-canonical type 2 immunity pathway diverges fundamentally from IL-4–driven responses, instead leveraging PU.1 collaboration for targeted gene regulation. The mechanistic elegance lies in DNA-PK (a DNA sensor) directly modifying STAT6 (an immune transducer) to activate repair—a rapid, integrated response to genotoxic stress. Indeed, our data suggest that DNA damage-induced Ser807 phosphorylation of STAT6 is primarily mediated by DNA-PK rather than other DDR kinases (e.g., ATM, ATR), highlighting its specificity in this pathway. However, given that DNA-PK can also be activated by self-DNA or viral DNA fragments in other immunological contexts[23, 24, 25], it will be important for future studies to explore whether additional kinases might phosphorylate STAT6 at Ser807 and what functions this modification may serve outside of the DNA damage response.

Notably, Ser807 phosphorylation represents a novel independent regulatory event, yet its function in modulating transcription is dependent on Tyr641 phosphorylation, the classical activation switch for STAT6. Ser807 phosphorylation creates a structural barrier that impedes RNF128 binding, suppressing K319 ubiquitination and proteasomal degradation. This extends STAT6's functional half-life, enabling

sustained DNA repair activity after damage—a safeguard against senescence. Beyond stabilizing STAT6, Ser807 phosphorylation licenses its partnership with PU.1. This macrophage-specific collaboration explains why STAT6 enhances DNA repair more robustly here than in other cells. PU.1, a pioneer factor, likely facilitates chromatin access at repair gene loci, while phospho-STAT6 provides stimulus-dependent recruitment. This model aligns with paradigms of lineage-determining and signal-dependent transcription factor synergy, here repurposed for senescence prevention.

Macrophages play a role in the immunosurveillance of senescent cells[16], and this phagocytic function is impaired in aged mice[51, 52, 53, 54, 55]. Loss of Ser807 phosphorylation triggers a vicious cascade: DNA repair deficiency results in senescence, which in turn impairs phagocytosis. *Stat6*$^{S807A/-}$ macrophages exhibited significant reduction in bacterial/senescent cell clearance, mirroring phagocytic defects in aged macrophages. This collapse in immunosurveillance permits accumulation of noxious agents and senescent cells, fueling tissue fibrosis and inflammaging. Crucially, adoptive transfer of Stat6$^{S807E/S807E}$ macrophages alleviates these deficits, positioning macrophage rejuvenation through enhanced immunosurveillance as a therapeutic strategy analogous to emerging senolytic CAR-T approaches[56, 57, 58].

In COPD patients—where aging intersects with environmental stress[8, 45]—we observed significant reductions in STAT6-Ser817 phosphorylation that correlated strongly with DNA damage and senescence markers. This pathway's disruption explains the accumulation of senescent macrophages in COPD lungs and aligns with the disease's hallmark sterile inflammation[59]. This may explain the limited clinical efficacy of IL4R blockade in COPD[60, 61]. In this case, IL4R blockade inhibits type 2 inflammation in pulmonary epithelial cells and smooth muscles to reduce COPD exacerbation. Counterproductively, it also inhibits macrophage DNA repair, which aggravates macrophage senescence and consequently

impairs senescent cell clearance to increase COPD exacerbation. Importantly, phosphomimetic STAT6 is sufficient to rescue repair and phagocytosis in human macrophages. This positions STAT6 Ser817 phosphorylation as both a candidate biomarker for pathological aging and a therapeutic target. Future studies could explore modulating this pathway (e.g., via DNA-PK activators or STAT6 phosphomimetics) to combat age-related diseases.

In summary, we delineate a linear DNA-PK–STAT6–PU.1 pathway that safeguards macrophage homeostasis. By reprogramming STAT6 into a damage-responsive stability switch, this pathway establishes a non-canonical type 2 immunity axis that counteracts senescence across molecular, cellular, and organismal levels. Its dysregulation in COPD underscores broad relevance; its amenability to therapeutic augmentation (e.g., phosphomimetic macrophages) offers new avenues to target age-related disease. While this study provides significant advances, the findings are based on experiments with limited sample sizes. Future studies should focus on validating these mechanisms in larger-scale preclinical animal models and exploring relevant genetic variations in large human cohorts.

Methods

Mice

Animal studies followed the protocols approved by the Institutional Animal Care and Use Committee (IACUC) of Peking University. All mice were housed at temperature (22 ± 1 °C) and humidity (60% ± 10%) controlled specific pathogen-free (SPF) environment under 12 h-12 h light-dark cycle, and provided with a normal diet (Xietong Shengwu, #1010063) and water ad libitum. Age and strain of mice were noted in the figure legends. Experimental/control animals were bred separately. *Cas9*$^{tg/+}$(026179, C57BL/6), *Stat6*$^{-/-}$ (005977, C57BL/6), *Sting*$^{-/-}$ (017537, C57BL/6) and *Lyz2*^{Cre} (004781, C57BL/6) mice were purchased from The Jackson Laboratories; *Stat6*$^{S807A/+}$ and *Stat6*$^{S807E/+}$ knock-in mice were generated by Cyagen Biosciences on C57BL/6 background by CRISPR/Cas9-mediated genome editing. *Stat6*$^{f/f}$ mice (T005778, C57BL/6) were from GemPharmatech, and CD45.1 (C57BL/6, JAX002014) mice from Laboratory Animal Resource Center of Tsinghua University. *Stat6*$^{-/-}$ mice were crossed with *Stat6*$^{S807A/+}$ or *Stat6*$^{S807E/+}$ ones to obtain *Stat6*$^{S807A/-}$ or *Stat6*$^{S807E/-}$ offspring. Isoflurane (RWD, #R510-22) was used to anesthetize mice. Male mice were used unless otherwise specified.

Human samples

Human lung samples were obtained from smokers with COPD, smokers without COPD and non-smoker controls, all receiving surgery for solitary lung tumors at Peking University Third Hospital. Lung tissues at maximum distance from the lesions and without tumor invasion or signs of obstructive pneumonia were collected by a pathologist. Characteristics of the study subjects are shown in Supplementary Table 1. The Ethics Committee of Peking University Third Hospital approved the study, and signed informed consent was obtained from all the study subjects.

Human fresh blood samples were collected from five healthy donors (four males and one female, 18-25 year-old), which were approved by the Ethical Committee on Human Research of Peking University (IRB00001052-25157), and all donors signed informed consent.

Generation of primary macrophages

Generation of bone marrow-derived macrophages (BMDM) was performed as previously described[13]. For isolation of peritoneal macrophage, 3% thioglycolate sodium medium was intraperitoneally injected into

male 8-12-week-old mice. After 3-day induction, peritoneal cavity was rinsed three times with 3 mL PBS. Then, precipitation of rinse solution was collected and plated in petri dishes. Macrophages were subsequently digested with 5 mM EDTA and cultured in DMEM supplemented with 10% fetal bovine serum (FBS) and 1% penicillin–streptomycin (P/S). For gene overexpression or gRNA-mediated deletion, cells were infected with AAV (DJ) (MOI: 400,000) for 24 h, then replaced with new medium and cultured for 48 h. For isolation of alveolar macrophages, bronchoalveolar lavage fluid (BALF) were collected from anesthetized (isoflurane) mice. The cells of BALF were washed by PBS, then plated in petri dishes with DMEM supplemented with 10% FBS and 1% P/S. After 2h culture, the cells were washed with PBS, and the adherent cells were considered as alveolar macrophages for further experiments.

For isolation of tissue F4/80+ macrophages, fresh tissues were cut into pieces and digested by 2 mg/mL type 1 collagenase, while Liberase for lung, with 10 U/mL DNase I in Hank's Balanced Salt Solution (HBSS) for 40 min at 37C. After lysis of red blood cells, the cell suspension was incubated with MACS anti-F4/80 beads (Miltenyi Biotec, #130-110-443) following the manufacturer's protocol. Double positive selected cells by LS column (Miltenyi Biotec, #130-042-401) were used as F4/80+ cells, and others were used as F4/80- cells.

Generation of primary human monocyte-derived macrophage was performed following previous protocol with slight modifications[62]. Briefly, peripheral blood mononuclear cells (PBMC) were isolated from fresh blood of healthy donors via Ficoll-Paque PLUS Media (GE Healthcare, # 17-1440-02) gradient. After wash by PBS, purified PBMCs were resuspended by PRMI 1640 (10% FBS, 2 mM L-glutamine and 1% P/S) and incubated in 37 °C 5% CO2 for 1.5 h. Removing unattached cells, the adherent cells (monocytes) were differentiated with PRMI 1640 supplemented with 50 ng/mL hM-CSF, 10% FBS, 2 mM L-glutamine and 1% P/S. After 5-day differentiation, the mature hMDMs were used for further experiments.

Cell culture and treatment

HEK 293T (CRL-3216), RAW 264.7 (TIB-71) and THP-1 (HIB-202) cells were obtained from the American Type Culture Collection. These cells, except THP-1 in PRMI 1640, were incubated in DMEM supplemented with 10% FBS and 1% P/S at 37 °C in a humidified 5% CO2 incubator. For differentiation of human macrophages, THP-1 cells were exposed to 100 ng/mL PMA (Sigma-Aldrich, #P1585) for 3 days. After pooled knock-out of STAT6 via lentivirus (selected by puromycin), THP-1 macrophages were

overexpressed STAT6 mutants via AAV method. For senescence induction, macrophages were treated with etoposide (5 μM, 12 h, Sigma-Aldrich, #E1383), then incubated in fresh complete culture medium for 3 days. For DNA repair assay, cells were challenged with 10 μM etoposide for 2h, then incubated in fresh medium for indicated time as a repair period. IL-4 (20 ng/mL, PeproTech, #214-14), DNA-PK inhibitor NU7026 (10 μM, Selleck Chemicals, #S2893), ATM inhibitor KU55933 (10 μM, Selleck Chemicals, #S1092), ATR inhibitor Berzosertib (0.5 μM, Selleck Chemicals, #S7102), CHK1/2 inhibitor AZD7762 (1 μM, Selleck Chemicals, #S1532), STAT6 inhibitor AS1517499 (2 μM, Selleck Chemicals, #S8685), STING inhibitor H151 (1 μM, Selleck Chemicals, #S6652), PTP1B inhibitor (2 μM, Santa Cruz, #sc-222227), PU.1 inhibitor DB2313 (10 nM, MedChem Express, #HY-124629), EPAC inhibitor ESI-09 (10μM, Selleck Chemicals, #S7499), hIL-4 (20 ng/mL, PeproTech, #200-04), LPS (100 ng/mL, Sigma-Aldrich, #L2630), IFNγ (20 ng/mL, PeproTech, #315-05) were used. For protein stability assay, cells were incubated with CHX (50 μg/mL, Sigma-Aldrich, #239763) for indicated time. Proteosome inhibitor MG132 (10 μg/mL, Selleck Chemicals, #S2619) and lysosome inhibitor Lys05 (10 μM, Selleck Chemicals, #S8369) were used. For detection of ROS level, probe DCFH-DA (10 μM, MedChem Express, #HY-D0940) was used.

Aging-related phenotype analysis

For evaluating physical fitness of mice, rotarod, hanging, treadmill and Y maze tests were performed as previously reported[13]. The details were as follows. For rotarod test, mice were trained on six-lane mouse rotarod (KEWBASIS, KW-6C) for two days before formal tests. The speed of rotarod started at 6 rpm, accelerated to 40 rpm within 5 min, maintained 40 rpm for 3 min, then accelerated to 60 rpm within 2 min, and maintained for 3 min. Twice for each mouse (with an interval over 15 min), and the better score was recorded. For hanging endurance test, mice were allowed to grab the wire with their forelimbs only. Scores were recorded as hanging maintenance (sec) × body weight (g), then averaged from 3 trials for each mouse. For treadmill test, mice were acclimatized to a treadmill for three consecutive days before formal tests. With 5° incline, mice ran at 10 m/min for the first 10 min, then 13 m/min for 5 min, and followed by increases of 2 m/min every 5 min until exhaustion defined by inability to remain on the treadmill for >5s. For Y maze exploration test, we performed as previously described[13]. Mice could freely explore three arms of Y maze in 10 min. The orders of arms explored were recorded. A complete

exploration (A-B-C) was considered as a correct selection. Bone density of mice was measured by Dual-energy X-ray absorptiometry (DXA, GE medical system).

Bleomycin-induced pulmonary fibrosis

For induction of pulmonary fibrosis, 3-month-old mice were anesthetized (isoflurane), then intranasally administered with 2 mg/kg bleomycin sulfate (Selleck Chemicals, #S1214) dissolved in 0.9% saline. Alveolar macrophages were collected from bronchoalveolar lavage fluid of mice 7 days after bleomycin treatment. Lung samples were collected 20 days after bleomycin treatment. For histological analysis, the collected lung samples were fixed in 4% paraformaldehyde over 24 h, dehydrated, and embedded in paraffin for sectioning. Paraffin sections (5 μm) were stained with hematoxylin and eosin, Masson's trichrome (Leagene, #DC0033), or Sirius red (Leagene, #DC0041) according to the manufacturers' instructions. Images were captured on an OLYMPUS BX51. The fibrosis scores were evaluated following a previous report[63]. For survival analysis, death or serious weight loss (30% loss) of mice was recorded at period of 40 days after bleomycin treatment. The mice with serious weight loss were euthanized by CO_2 exposure.

Transfer of macrophages

BMDMs with indicated genotypes were generated. Then, mature BMDMs were digested, resuspended, calculated, and diluted. To determine the optimal number of macrophages for transfer, we compared mRNA expression of senescence markers in eWAT from *Stat6*$^{f/f}$;*Lyz2*^{Cre} mice that received the indicated BMDMs. For final transfer, about 2×10^6 BMDMs were transferred to anesthetized (isoflurane) recipient mice via retro-orbital injection each 5 weeks. The phenotypes of recipient mice were analyzed 5 weeks after second transfer.

To compare *in vivo* homeostasis of macrophages in Fig. 5H and 5I. Resident PMs were isolated from mice with indicated genotypes by MACS anti-F4/80 beads (Miltenyi Biotec). These resident PMs were cultured in medium (5 ng/mL M-CSF, 15% FBS in PRMI-1640), then transfected with marker proteins (mCherry or GFP) via AAV. 3 days after transfection, labeled cells were recorded labeling efficiency and counted. Equal number of resident-PMs (three different genotypes) were mixed well. 2×10^6 mixed resident-PMs were suspended with PBS, and intraperitoneally injected into one CD45.1 mouse. 14 days after transfer,

the peritoneal cells were collected from recipient mice and more than 8×10^5 CD45.2+ cells were obtained and further analyzed by flow cytometry.

For transfer of alveolar macrophages, anesthetized CD45.1+ mice were transferred 1×10^5 BALF AMs with indicated genotypes in 100 μL PBS by intratracheal instillation. 2 days after transfer, recipient mice were challenged with bleomycin to induce pulmonary fibrosis.

TurboID

TurboID is performed as previously described[64]. Briefly, cells expressed with STAT6-Turbo-Flag or Turbo-Flag were incubated with 50 μM biotin (Sigma-Aldrich, #B4501) for 10 min after Eto treatment. The labeling was stopped by transferring cells onto ice and washing five times with ice-cold PBS. Then the cells were lysed by RIPA buffer with protease cocktail inhibitors, and the biotinylated proteins were enriched by streptavidin magnetic beads (Thermo Fisher, #88816) with rotation at 4 ℃ overnight. The biotinylated protein was detected by immunoblot.

Mass spectrometry

To identify potential phosphorylation sites of STAT6, RAW 264.7 cells were overexpressed with STAT6-HA. 48 hours after transfection, cells were treated with 10 μM etoposide for 2 h, then lysed for immunoprecipitation using anti-HA beads (Thermo Fisher, #88836). Immunoprecipitates were separated by SDS–PAGE and then Coomassie blue staining was carried out. Bands of interest were cut from the gel and then in-gel digestion was performed using sequencing grade-modified trypsin. The peptides (1 sample in control group and 1 in Eto group) were analyzed by liquid chromatography–tandem mass spectrometry (LC–MS/MS) with nano-LC combined with Orbitrap Q Exactive mass spectrometer. The MS/MS spectra from each LC–MS/MS run were searched against the selected database using the Proteome Discoverer searching algorithm (v1.4). The phosphopeptides were further verified using the phosphoRS 3.1 node in Proteome Discoverer software. All MS/MS spectra corresponding to phosphopeptides were manually examined. The detail of peptides was listed in Supplementary Data 1 & 2.

Constructs

Mouse *Rnf128*, *Cblb*, *Ptpn1*, *Ptpn2* and *Shp1* cDNAs were cloned from BMDM cDNA, and human *STAT6* was cloned from THP-1 cDNA. Mouse *Stat6*(S807A), *Stat6*(S807E) and human *STAT6*(S817A) and *STAT6*(S817E) were generated by one-step PCR mutagenesis and verified by DNA sequencing. TurboID plasmid was gifted from Dr. Wei Qin (Tsinghua University). Dual luciferase reporter of STAT6 (4×S6 reporter) (#35554) and DNA repair reporter plasmids[65] (#98896, #98895, #26477) were obtained from Addgene. Dual luciferase reporter of *Ube2t*-promoter was used as previous study[13]. For expression in Thio-PMs and THP-1 cells, recombinant adeno-associated viruses (AAVs) were used. For expression in other cells, plasmids were transinfected via Lipo8000 (Beyotime, #C0533). For guide RNA plasmid construction, the indicated 20 bp gRNA was inserted into pAAV-U6-sgRNA-CMV-GFP vector (Addgene, #85451)[66] or lentiCRISPR v2 vector (Addgene, #52961)[67]. gRNAs were designed by CRISPick[68]. The gRNAs sequences used in this study were listed in Supplementary Table 2.

Immunoblot and immunoprecipitation

Cells or frozen tissue samples were lysed in RIPA buffer with protease cocktail inhibitors. Lysate was separated by SDS-PAGE and transferred to nitrocellulose or PVDF membrane (Millipore) following standard protocols. For immunoprecipitation, cells were lysed in immunoprecipitation lysis buffer (50 mM Tris-HCl pH 8.0, 120 mM NaCl, 10% glycerol, 1% NP-40, 5 mM EDTA and cocktail protease inhibitors) for 1 h at 4 °C. And supernatant of cell lysate was incubated with anti-HA magnetic beads or anti-Flag agarose beads (Smart-Lifesciences, #SA042001) for 2h at 4 °C. For endogenous immunoprecipitation experiments, supernatant of cell lysate was incubated with indicated primary antibody at 4 °C overnight. Then rProtein A/G Beads (Cell Signaling, # 37478) were added and incubated for 4 h. The immunoprecipitated was washed three times with buffer and followed by immunoblot. Antibodies used were as follows: HSP90 (Santa Cruz, #sc-13119, 1:10,000), α-Tubulin (Sigma, #T6199, 1:10,000), STAT6 (Cell Signaling, #5397, 1:1500), pSTAT6(pY641) (Cell Signaling, #56554, 1:1000), pSTAT6(pS807) (ABclonal Tech, customized, 1:200), DNA-PK (Santa Cruz, #sc-390849, 1:500), ATM (Cell Signaling, #2873, 1:1000), ATR (Santa Cruz, #sc-515173, 1:500), CHK1 (Cell Signaling, #2360, 1:1500), CHK2 (Proteintech, #13954-1-AP, 1:1000), p16-INK4A (Abcam, #ab211542, 1:1000), γH2AX (Cell Signaling, #9718, 1:1500), BRCA1 (Thermo Fisher, #MA1-23164, 1:1000), UBE2T (Thermo Fisher, #PA576202, 1:1000), JAK (Cell Signaling, #50996, 1:1000), STING (Cell Signaling, #13647,

1:2000), STING (pS365) (Cell Signaling, #72971, 1:1000), pTBK1 (pS172) (Cell Signaling, #5483, 1:1000), pJAK1 (pY1034/1035) (Cell Signaling, #74129, 1:1000), Ubiquitin (Cell Signaling, #3936, 1:1000), K48-specific ubiquitin (Abcam, #ab140601, 1:1000), PU.1 (Abcam, #ab227835, 1:1500), Col1a1 (Cell Signaling, #72026, 1:1000), SMAD2/3 (Cell Signaling, #8685, 1:1000), p-SMAD2 (Ser465/467)/SMAD3 (Ser423/425) (Cell Signaling, #8828, 1:1000), αSMA (Cell Signaling, #19245, 1:2000) anti-HA (Cell Signaling, #3724, 1:5000) and anti-Flag (Cell Signaling, #8146, 1:5000).

Generation of STAT6 pS807-sepicific antibody

To generate a polyclonal antibody specific for STAT6 phosphorylated at Ser807 (pS807), we collaborated with ABclonal Tech. Inc. Briefly, KLH-conjugated mouse STAT6 peptides (residues 802-816) were synthesized, corresponding to both the non-phosphorylated form and the form phosphorylated at Ser807. These purified peptides were used to immunize SPF rabbits over five rounds. The immunization dosage was 0.35 mg per injection, with the first injection being 0.7 mg. Prior to the fifth immunization, serum was collected from the immunized rabbits and validated for its ability to specifically recognize pS807-STAT6. The rabbit whose serum demonstrated the best efficacy and specificity was selected for the final immunization, after which the serum was collected and the polyclonal antibody was purified. The validation data for the STAT6 pS807-specific antibody is presented in Supplementary Fig. 2E.

Proximity ligation assay

Proximity ligation assay was performed with PLA In Situ Red Starter Kit (Sigma Aldrich, #DUO92101) following manufacturer's protocol. Briefly, PMs post 2-h Eto (or IL-4) treatment were fixed by 4% PFA for 15 min at 22℃, washed three times with PBS and permeabilized with 0.2% Triton X-100 in PBS for 10 min. After incubation with blocker at 37℃ for 1 h, cells were incubated with primary antibodies with recommended dilution at 4℃ overnight. Next day, the PLUS and MINUS probes were added for 1 h at 37℃. After 30 min ligation at 37℃, amplification was carried out for 100 min at 37℃. Cells were washed four times, then incubated with DAPI. Images were captured by Nikon AXR microscope.

Immunofluorescence

After indicated treatment, cells were washed twice with ice-cold PBS, then fixed with 4% PFA for 15 min at 22℃, washed three times with PBS and permeabilized with 0.2% Triton X-100 in PBS for 10 min. Cells were blocked in PBS containing 5% BSA for 30 min at 22℃, and then incubated in PBS containing primary antibodies with recommended dilution at 4℃ overnight. Next day, the cells were rinsed and incubated with secondary antibodies in PBS (1:1000) for 1 h at 22℃. After wash, the nuclei were counterstained with DAPI. Cells were imaged using Nikon AXR microscope.

Quantitative RT-PCR

Total RNA was isolated from tissues or cells using TRIzol reagent (Sigma-Aldrich, #T9424). And reverse transcription was carried out using HiScript III RT SuperMix (Vazyme, # R323-01) and qPCR reaction was carried out using ChamQ SYBR qPCR master mix (Vazyme, # Q311-02) on ABI StepOnePlus (Thermo Fisher). Relative mRNA expression was calculated via $2^{(-\Delta\Delta CT)}$ method. *36B4* (*Rplp0*) was used as an internal control for mouse samples, and GAPDH for human samples. Primer sequences are summarized in Supplementary Table 2.

CUT&Tag

CUT&Tag was performed using Hyperactive Universal CUT&Tag Assay Kit (Vazyme, #TD903) according to the manufacturer's protocol. Briefly, after indicated treatment, PMs were digested and collected. For ConA bead binding, cells were incubated at 4°C overnight with primary antibody. After 3-time washes, cells were incubated with secondary antibody for 1h at 22 °C. Then cells were incubated with pG-Tnp to get target DNA fragments followed by DNA extraction. Obtained DNA was amplified by PCR, using adaptor primers: F: TCGTCGGCAGCGTCAGATGTGTATAAGAGACAG, R: GTCTCGTGGGCTCGGAGATGTGTATAAGAGACAG. Purified products were used to detect relative enrichment of targeted DNA fragments, while total nuclear DNA of pellets was used as input. The primer pairs were listed in Supplementary Table 2.

SA-βGal staining

SA-βGal staining was performed using Senescence β-Galactosidase Staining Kit (Beyotime, #C0602) according to the manufacturer's protocols. For eWAT staining, fresh eWAT was cut into 1~2 cm^3 pieces,

then fixed by 4% PFA for 20 min. The fixed eWAT pieces were incubated in staining buffer at 37℃ for 8 h. After 3-day wash by PBS, images were captured.

Lipofuscin staining

Lipofuscin staining was performed as a previous report[69]. 3% H_2O_2 was used as oxidant blocker. SenTraGor Cell Senescence Reagent (GL13, Cayman Chemical, #35568) was used for staining.

Phagocytosis assay

For *in vitro* phagocytosis assay of macrophages, Phagocytosis Assay Kit (IgG FITC) (Cayman Chemical, #500290) was used following manufacturer's protocols. For *in vivo* phagocytosis assay, E. coli and senescent MEFs were used. Simply, 1×10^7 colony-forming units E. coli were injected into peritoneum of mice. After 24 h, the ascites was collected, and the bacteria burden was calculated by spread plate method. On the other hand, senescence was induced with Eto in MEFs expressing mCherry, then 5×10^6 senescent MEFs were intraperitoneally injected into mice. After 3 days, the remained senescent MEFs ($mCherry^+$) were analyzed by flow cytometry.

Bioinformatic analysis

For our original RNA-seq dataset, cleaned reads were aligned to a mouse genome (mm10) using HISAT2 (v2.1.0), then read counts were extracted by Subread (FeatureCounts, v2.0.1). Gene expression was calculated by DESeq2 (v2.11.40.6) in R. Principal component analysis was performed by DESeq2 (v2.11.40.6) in R. Gene set enrichment analysis was performed by GSEA software (v4.3.2) with recommended settings. For human sample analysis, we downloaded the RNA-seq datasets from GTEx v8.0[44] (https://www.gtexportal.org/). Raw data was converted into transcripts per kilobase million (TPM) as presented data. And gene expression correlation analysis was performed by Spearman correlation. The ChIP-seq datasets of murine macrophages were obtained from GSE38377 (PU.1)[70]. For prediction of transcriptional factors, the sequences of promoters (*Brca1* (TSS -2900 bp to +100 bp) and *Ube2t* (TSS -2400 bp to +100 bp)) were loaded into AnimalTFDB v4.0[39] with default setup. TFs with high score (> 10) was subsequently analyzed. The expression of TFs in different cell types was determined by RNA-seq datasets, and genes with over 0.5 TPM were considered as expressed TFs. To assess *Spi1* expression

across cell types, we reanalyzed publicly available mouse adipose tissue single-cell sequencing data (Li et al. 2021[41], SCP708) from Single Cell Portal database[71].

Quantification and statistical analysis

The number of mice or samples per group, replicates of independent experiments and statistical tests are presented in the legends. Sample size was chosen based on previous experiments or based on pilot experiments to ensure the possibility of statistical analysis and to minimize the use of experimental animals based on the 3R principles[4, 13]**.** Data are showed as means ± s.e.m. and analyzed by GraphPad Prism 9. The statistical methods are indicated in the figure legends.

Data availability

This paper does not report original code. The original RNA-seq datasets of Thio-PMs is available from GEO (GSE278458, https://www.ncbi.nlm.nih.gov/geo/query/acc.cgi?acc=GSE278458). The ChIP-seq dataset of macrophages (PU.1) are obtained from GSE38377 (https://www.ncbi.nlm.nih.gov/geo/query/acc.cgi). The mass spectrometry proteomics data have been deposited to the ProteomeXchange Consortium via the iProX partner repository with the dataset identifier PXD074331(https://proteomecentral.proteomexchange.org/cgi/GetDataset?ID=PXD074331).

All materials generated in this study, including stable cell lines and newly developed pSTAT6 antibodies for mouse and human, will be made available upon request.

Source data are provided with this paper.

References

1. Takeuchi O, Akira S. Pattern Recognition Receptors and Inflammation. *Cell* **140**, 805-820 (2010).

2. Chen GY, Nuñez G. Sterile inflammation: sensing and reacting to damage. *Nat Rev Immunol* **10**, 826-837 (2010).

3. López-Otín C, Blasco MA, Partridge L, Serrano M, Kroemer G. Hallmarks of aging: An expanding universe. *Cell* **186**, 243-278 (2023).

4. Yousefzadeh MJ, *et al.* An aged immune system drives senescence and ageing of solid organs. *Nature* **594**, 100-105 (2021).

5. Franceschi C, *et al.* Inflamm-aging -: An evolutionary perspective on immunosenescence. *Ann Ny Acad Sci* **908**, 244-254 (2000).

6. Gulen MF, *et al.* cGAS-STING drives ageing-related inflammation and neurodegeneration. *Nature* **620**, 374-380 (2023).

7. Minhas PS, *et al.* Restoring metabolism of myeloid cells reverses cognitive decline in ageing. *Nature* **590**, 122-128 (2021).

8. Schneider JL, Rowe JH, Garcia-de-Alba C, Kim CF, Sharpe AH, Haigis MC. The aging lung: Physiology, disease, and immunity. *Cell* **184**, 1990-2019 (2021).

9. Santoro A, Bientinesi E, Monti D. Immunosenescence and inflammaging in the aging process: age-related diseases or longevity. *Ageing Res Rev* **71**, 101422 (2021).

10. He SH, Sharpless NE. Senescence in Health and Disease. *Cell* **169**, 1000-1011 (2017).

11. Moiseeva V, *et al.* Senescence atlas reveals an aged-like inflamed niche that blunts muscle regeneration. *Nature* **613**, (2023).

12. Liu J-Y, *et al.* Cells exhibiting strong p16 INK4a promoter activation in vivo display features of senescence. *Proceedings of the National Academy of Sciences* **116**, 2603-2611 (2019).

13. Zhou Z, *et al.* Type 2 cytokine signaling in macrophages protects from cellular senescence and organismal aging. *Immunity* **57**, 513-527 (2024).

14. Franceschi C, Garagnani P, Vitale G, Capri M, Salvioli S. Inflammaging and 'Garb-aging'. *Trends Endocrin Met* **28**, 199-212 (2017).

15. Park MD, Silvin A, Ginhoux F, Merad M. Macrophages in health and disease. *Cell* **185**, 4259-4279 (2022).

16. Sturmlechner I, *et al.* p21 produces a bioactive secretome that places stressed cells under immunosurveillance. *Science* **374**, eabb3420 (2021).

17. Van Dyken SJ, Locksley RM. Interleukin-4- and Interleukin-13-Mediated Alternatively Activated Macrophages: Roles in Homeostasis and Disease. *Annual Review of Immunology* **31**, 317-343 (2013).

18. Czimmerer Z, *et al.* The Transcription Factor STAT6 Mediates Direct Repression of Inflammatory Enhancers and Limits Activation of Alternatively Polarized Macrophages. *Immunity* **48**, 75-+ (2018).

19. Piccolo V, *et al.* Opposing macrophage polarization programs show extensive epigenomic and transcriptional cross-talk. *Nature Immunology* **18**, 530-540 (2017).

20. Chen HH, *et al.* Activation of STAT6 by STING Is Critical for Antiviral Innate Immunity. *Cell* **147**, 436-446 (2011).

21. Schumacher B, Pothof J, Vijg J, Hoeijmakers JHJ. The central role of DNA damage in the ageing process. *Nature* **592**, 695-703 (2021).

22. Blackford AN, Jackson SP. ATM, ATR, and DNA-PK: The Trinity at the Heart of the DNA Damage Response. *Mol Cell* **66**, 801-817 (2017).

23. Ferguson BJ, Mansur DS, Peters NE, Ren HW, Smith GL. DNA-PK is a DNA sensor for IRF-3-dependent innate immunity. *Elife* **1**, (2012).

24. Burleigh K, *et al.* Human DNA-PK activates a STING-independent DNA sensing pathway. *Sci Immunol* **5**, (2020).

25. Wang Y, *et al.* Cytoplasmic DNA sensing by KU complex in aged $CD4^+$ T cell potentiates T cell activation and aging-related autoimmune inflammation. *Immunity* **54**, 632-+ (2021).

26. Stark GR, Darnell JE. The JAK-STAT Pathway at Twenty. *Immunity* **36**, 503-514 (2012).

27. Miller KN, *et al.* Cytoplasmic DNA: sources, sensing, and role in aging and disease. *Cell* **184**, 5506-5526 (2021).

28. Yue XQ, Bai CJ, Xie DF, Ma T, Zhou PK. DNA-PKcs: A multi-faceted player in DNA damage response. *Front Genet* **11**, 607428 (2020).

29. Wang CW, *et al.* GPS 5.0: An Update on the Prediction of Kinase-specific Phosphorylation Sites in Proteins. *Genom Proteom Bioinf* **18**, 72-80 (2020).

30. Huston E, *et al.* EPAC and PKA allow cAMP dual control over DNA-PK nuclear translocation. *P Natl Acad Sci USA* **105**, 12791-12796 (2008).

31. Sahoo A, Alekseev A, Obertas L, Nurieva R. Grail controls Th2 cell development by targeting STAT6 for degradation. *Nat Commun* **5**, 4732 (2014).

32. Qiao GL, *et al.* E3 Ubiquitin Ligase Cbl-b Suppresses Proallergic T Cell Development and Allergic Airway Inflammation. *Cell Reports* **6**, 709-723 (2014).

33. Wang CW, *et al.* GPS-Uber: a hybrid-learning framework for prediction of general and E3-specific lysine ubiquitination sites. *Brief Bioinform* **23**, bbab574 (2022).

34. Yu K, *et al.* qPTM: an updated database for PTM dynamics in human, mouse, rat and yeast. *Nucleic Acids Res* **51**, D479-D487 (2023).

35. Shi JH, *et al.* TRAF3/STAT6 axis regulates macrophage polarization and tumor progression. *Cell Death and Differentiation* **30**, 2005-2016 (2023).

36. Hanson EM, Dickensheets H, Qu CK, Donnelly RP, Keegan AD. Regulation of the dephosphorylation of Stat6 -: Participation of TYR-713 in the interleukin-4 receptor α, the tyrosine phosphatase SHP-1, and the proteasome. *J Biol Chem* **278**, 3903-3911 (2003).

37. Lu XQ, *et al.* PTP1B is a negative regulator of interleukin 4-induced STAT6 signaling. *Blood* **112**, 4098-4108 (2008).

38. Lu XQ, *et al.* T-cell protein tyrosine phosphatase, distinctively expressed in activated-B-cell-like diffuse large B-cell lymphomas, is the nuclear phosphatase of STAT6. *Mol Cell Biol* **27**, 2166-2179 (2007).

39. Shen WK, *et al.* AnimaITFDB 4.0: a comprehensive animal transcription factor database updated with variation and expression annotations. *Nucleic Acids Res* **51**, D39-D45 (2023).

40. Rosenbauer F, Tenen DG. Transcription factors in myeloid development: balancing differentiation with transformation. *Nat Rev Immunol* **7**, 105-117 (2007).

41. Li J, *et al.* Neurotensin is an anti-thermogenic peptide produced by lymphatic endothelial cells. *Cell Metab* **33**, 1449-+ (2021).

42. Aegerter H, Lambrecht BN, Jakubzick C. Biology of lung macrophages in health and disease. *Immunity* **55**, 1564-1580 (2022).

43. Mertins P, *et al.* Proteogenomics connects somatic mutations to signalling in breast cancer. *Nature* **534**, 55-62 (2016).

44. Aguet F, *et al.* The GTEx Consortium atlas of genetic regulatory effects across human tissues. *Science* **369**, 1318-1330 (2020).

45. Christenson SA, Smith BM, Bafadhel M, Putcha N. Chronic obstructive pulmonary disease. *Lancet* **399**, 2227-2242 (2022).

46. Prieto LI, *et al.* Senescent alveolar macrophages promote early-stage lung tumorigenesis. *Cancer Cell* **41**, 1261-1275 (2023).

47. Haston S, *et al.* Clearance of senescent macrophages ameliorates tumorigenesis in KRAS-driven lung cancer. *Cancer Cell* **41**, 1242-1260 (2023).

48. Mittelbrunn M, Kroemer G. Hallmarks of T cell aging. *Nature Immunology* **22**, 687-698 (2021).

49. Desdín-Micó G, *et al.* T cells with dysfunctional mitochondria induce multimorbidity and premature senescence. *Science* **368**, 1371-1376 (2020).

50. Kawamoto S, *et al.* Bacterial induction of B cell senescence promotes age-related changes in the gut microbiota. *Nat Cell Biol* **25**, 865-876 (2023).

51. Linehan E, Dombrowski Y, Snoddy R, Fallon PG, Kissenpfennig A, Fitzgerald DC. Aging impairs peritoneal but not bone marrow-derived macrophage phagocytosis. *Aging Cell* **13**, 699-708 (2014).

52. Blacher E, *et al.* Aging disrupts circadian gene regulation and function in macrophages. *Nature Immunology* **23**, 229-236 (2022).

53. Pluvinage JV, *et al.* CD22 blockade restores homeostatic microglial phagocytosis in ageing brains. *Nature* **568**, 187-192 (2019).

54. Li ZG, *et al.* Aging-Impaired Filamentous Actin Polymerization Signaling Reduces Alveolar Macrophage Phagocytosis of Bacteria. *J Immunol* **199**, 3176-3186 (2017).

55. Zhao H, *et al.* Identifying specific functional roles for senescence across cell types. *Cell* **187**, 7314-7334.e7321 (2024).

56. Amor C, *et al.* Senolytic CAR T cells reverse senescence-associated pathologies. *Nature* **583**, 127-132 (2020).

57. Yang D, *et al.* NKG2D-CAR T cells eliminate senescent cells in aged mice and nonhuman primates. *Sci Transl Med* **15**, eadd1951 (2023).

58. Amor C, *et al.* Prophylactic and long-lasting efficacy of senolytic CAR T cells against age-related metabolic dysfunction. *Nature Aging* **4**, 336-349 (2024).

59. Xu J, Zeng QY, Li SQ, Su QL, Fan H. Inflammation mechanism and research progress of COPD. *Front Immunol* **15**, (2024).

60. Bhatt SP, *et al.* Dupilumab for chronic obstructive pulmonary disease with type 2 inflammation: a pooled analysis of two phase 3, randomised, double-blind, placebo-controlled trials. *Lancet Resp Med* **13**, 234-243 (2025).

61. Bhatt SP, *et al.* Dupilumab for COPD with Blood Eosinophil Evidence of Type 2 Inflammation. *New Engl J Med* **390**, 2274-2283 (2024).

62. Bernaerts E, Vandooren J. Protocol to generate human monocyte-derived macrophages in the absence of exogenous proteases and protease inhibitors to study proteolysis. *STAR Protoc* **6**, 103826 (2025).

63. Huebner RH, *et al.* Standardized quantification of pulmonary fibrosis in histological samples. *Biotechniques* **44**, 507-514 (2008).

64. Qin W, *et al.* Dynamic mapping of proteome trafficking within and between living cells by TransitID. *Cell* **186**, 3307-3324 (2023).

65. Arnoult N, *et al.* Regulation of DNA repair pathway choice in S and G2 phases by the NHEJ inhibitor CYREN. *Nature* **549**, 548-552 (2017).

66. Duan YJ, Ma GE, Huang XG, D'Amore PA, Zhang F, Lei HT. The clustered, regularly interspaced, short palindromic repeats-associated endonuclease 9 (CRISPR/Cas9)-created T309G mutation enhances vitreous-induced expression of MDM2 and proliferation and survival of cells. *J Biol Chem* **291**, 16339-16347 (2016).

67. Sanjana NE, Shalem O, Zhang F. Improved vectors and genome-wide libraries for CRISPR screening. *Nat Methods* **11**, 783-784 (2014).

68. Sanson KR, *et al.* Optimized libraries for CRISPR-Cas9 genetic screens with multiple modalities. *Nat Commun* **9**, (2018).

69. Evangelou K, *et al.* Robust, universal biomarker assay to detect senescent cells in biological specimens. *Aging Cell* **16**, 192-197 (2017).

70. Ostuni R, *et al.* Latent Enhancers Activated by Stimulation in Differentiated Cells. *Cell* **152**, 157-171 (2013).

71. Tarhan L, Bistline J, Chang J, Galloway B, Hanna E, Weitz E. Single Cell Portal: an interactive home for single-cell genomics data. *bioRxiv*, (2023).

Acknowledgements

We thank members of the Qiu laboratory for comments on the manuscript. We are grateful to the Flow Cytometry Core of National Center for Protein Sciences and the Core Facilities of Life Sciences at Peking University for assistance with flow cytometry and confocal microscopy. We also thank Ms. Meng Han in the Proteomics Facility at Tsinghua University Technology Center for Protein Sciences for mass spectrometry analysis of protein modification. This work was supported by grants from National Key

R&D Program of Ministry of Science and Technology of the People's Republic of China (2024YFA1802103, 2021YFA0804801 and 2018YFA0800702) to Y.Q.

Author contributions

Z.Z. designed and performed the main experiments with assistance from X.L., Y.W., L.L., C.W.; Z.Z., Y.S., D.W. and Y.Q. discussed and interpreted the results from the study; Z.Z., D.W. and Y.Q. conceived, supervised, and wrote the paper.

Competing Interests

Authors declare that they have no competing interests.

Figure Legends

Figure 1: Elevated activation of STAT6 upon DNA damage.

(**A**) Immunoblots of pSTAT6 (pY641) and γH2AX in thioglycolate-elicited peritoneal macrophages (Thio-PM) with Etoposide (Eto) and IL-4 treatment. Right panel shows the relative intensity of pSTAT6 (pY641) (*n* = 4 independent experiments).

(**B**) Immunofluorescence images of staining (pSTAT6 (pY641), red; DAPI, blue) of IL-4-stimulated Thio-PMs treated with Eto. Scale bars 50 μm. Right panel shows the quantification of pSTAT6 (pY641) (*n* = 3 biological replicates per group).

(**C**) Immunoblots of pSTAT6 (pY641) and γH2AX in Eto-treated Thio-PMs with different inhibitors. KU55933, inhibitor of ATM. Berzosertib, inhibitor of ATR. NU7026, inhibitor of DNA-PK. AZD7762, inhibitor of CHK1/2. Right panel shows the quantification of pSTAT6 (pY641) (*n* = 3 independent experiments).

(**D**) Immunoblots of pSTAT6 (pY641) and γH2AX in Eto-treated *Cas9*$^{tg/+}$ Thio-PMs with indicated sgRNA. Right panel shows the quantification of pSTAT6 (pY641)/tSTAT6 (*n* = 3 independent experiments).

(**E**) Dual luciferase reporter of STAT6 in RAW 264.7 cells treated with Eto and NU7026 (*n* = 3 per group). Data are mean ± s.e.m. p-value was calculated by paired two-tailed Student's *t*-test (A, D), unpaired two-tailed Student's *t*-test (B), one-way ANOVA with Dunnett's correction (C, E).

Figure 2: DNA-PK phosphorylates STAT6 at Ser807.

(**A**) Co-IP of STAT6-Turbo and JAK1, DNA-PK, ATM, ATR in RAW 264.7 cells with TurboID.

(**B**) Proximity ligation assay (PLA) of STAT6 and DNA-PK in Thio-PMs treated with Eto. Scale bars 10 μm.

(**C**) The quantification of PLA signal in (B) (*n* = 3 biological replicates per group, with more than 100 cells).

(**D**) Diagram of phosphorylated sites in mouse STAT6 after Eto treatment.

(**E**) Immunoblots of pSTAT6 (pY641) and tSTAT6 in *Stat6*$^{-/-}$ Thio-PMs expressing STAT6 mutants (WT, S807A, S807E).

(**F**) Immunoblots of pSTAT6 (pY641) in STAT6-mutants-expressed *Cas9*$^{tg+}$ Thio-PMs with *Prkdc* sgRNA under IL-4 & Eto co-treatment.

(**G**) Dual luciferase reporter of STAT6 in RAW 264.7 cells expressing STAT6 mutants under IL-4 treatment (*n* = 3 biological replicates per group).

(**H**) Immunoblots of pSTAT6 (pS807) and γH2AX in Eto-treated *Cas9*$^{tg+}$ Thio-PMs with *Prkdc* sgRNAs.

(**I**) Immunoblots of pSTAT6 (pS807) and γH2AX in Eto-treated *Cas9*$^{tg/+}$ Thio-PMs with *Ku70* or *Ku80* sgRNA.

(**J**) Immunoblots of pSTAT6 (pS807) and γH2AX in Eto-treated Thio-PMs pre-treated with NU7026. Right panel shows the relative intensity of pSTAT6 (pS807) (*n* = 3 independent experiments).

(**K**) Immunoblots of pSTAT6 (pS807) and pSTAT6 (pY641) in Thio-PMs with indicated treatment. AS1517499, an inhibitor of STAT6 (block of pY641).

(**L**) Immunoblots of pSTAT6 (pS807) and tSTAT6 in Eto-treated *Stat6*$^{-/-}$ Thio-PMs expressing STAT6 mutants (WT, Y641F).

The blot results are representative of three biologically independent repeats in (A, E, F, H, I, K and L). Data are mean ± s.e.m. Unpaired two-tailed Welch's *t*-test (C), One-way ANOVA with Dunnett's correction (G), paired two-tailed Student's *t*-test (J).

Figure 3: Ser807 phosphorylation attenuates activated-STAT6 degradation.

(**A**) Hypothetical model of regulation of pSTAT6 (pY641).

(**B**) Immunoblots of pSTAT6 (pY641) and tSTAT6 in STAT6-mutants (WT, S807E)-expressed RAW 264.7 cells under IL-4 stimulation for 30 min or 4 h.

(**C**) Quantification of pSTAT6 (pY641)/tSTAT6 in (B) (n = 3 independent experiments).

(**D**) Stabilization assay of STAT6 mutants (WT, S807E) in IL-4-stimulated RAW 264.7 cells under CHX treatment.

(**E**) Degradation curve of pSTAT6 (pY641) in (D) (n = 3 independent experiments).

(**F**) Immunoblots of pSTAT6 (pY641) and tSTAT6 in MG132-pre-treated *Stat6*$^{-/-}$ PMs expressing STAT6 mutants (WT, S807E) under IL-4 stimulation for 4h.

(**G**) Immunoblots of ubiquitination and K48-ubiquitination on STAT6 in Thio-PMs with indicated treatments. The bottom right panel shows the quantification of STAT6 ubiquitination (n = 3 independent experiments).

(**H**) Co-IP of RNF128-FLAG with STAT6-HA mutants (WT, S807E) in RAW 264.7 cells after 4-h IL-4 stimulation.

(**I**) The quantification of the interaction between STAT6 and RNF128 in (H) (n = 4 independent experiments).

(**J**) Immunoblots of ubiquitination on STAT6-HA mutants (WT, S807E) and their interaction with RNF128-FLAG in RAW 264.7 cells after 4-h IL-4 stimulation.

(**K**) Immunoblots of ubiquitination on STAT6-HA mutants (WT, K319R, K595R, K319R/K595R) in RAW 264.7 cells after 4-h IL-4 stimulation.

(**L**) Stability assay of STAT6 mutants (WT, K319R, K595R) in RAW 264.7 cells under CHX treatment.

(**M**) Stability assay of STAT6 mutants (WT, S807A, S807A/K319R) in RAW 264.7 cells under CHX treatment.

(**N**) Diagram of pS807 effect on activated STAT6 stability.

The blot data are representative of three independent repeats (F and J–M). Data are mean ± s.e.m. Paired two-tailed *t*-test (C, I), ordinary two-way ANOVA (E), one-way ANOVA with Dunnett's correction (G).

Figure 4: Ser807-phosphorylated STAT6 promotes DNA repair in macrophages.

(**A**) Principal component (PC) analysis plot of Thio-PMs from *Stat6*$^{WT/WT}$, *Stat6*$^{S807A/S807A}$ and *Stat6*$^{S807E/S807E}$ mice, calculated by DESeq2.

(**B**) Gene set enrichment analysis (GSEA) in pathways "Recatome_DNA_Repair", "Hallmark_Inflammatory_response" and "SAUL_SEN_MAYO", compared *Stat6*$^{S807E/S807E}$ with *Stat6*$^{S807A/S807A}$ Thio-PMs, calculated by GSEA (v4.3.2).

(**C**, **D**) DNA repair capacity of Thio-PMs from *Stat6*$^{WT/-}$, *Stat6*$^{S807A/-}$ and *Stat6*$^{S807E/-}$ mice. The representative images of immunofluorescence staining (γH2AX, red; DAPI, blue) of PMs (C), and the quantifications (γH2AX positive proportions and mean fluorescence intensity (MFI)) are showed in (D) (n = 3 biological replicates per group). Scale bars 100 μm.

(**E**) STAT6 CUT&Tag binding enrichment of Thio-PMs from *Stat6*$^{WT/-}$, *Stat6*$^{S807A/-}$ and *Stat6*$^{S807E/-}$ mice after IL-4 treatment (n = 3 biological replicates per group), which was assessed by qPCR. B1/B2/B3, three STAT6-binding sties around *Brca1* locus. U, three STAT6-binding sties around *Ube2t* locus.

(**F**) Diagram of transcription co-factors screening. TFs regulating *Brca1* or *Ube2t* were predicted by AnimalTFDB 4.0 and their expression was analyzed by RNA-seq (TPM > 0.5).

(**G**) Endogenous Co-IP of STAT6 and PU.1 in Thio-PMs co-treated with Eto and IL-4 for 2h.

(**H**) PLA of STAT6 and PU.1 in Thio-PMs co-treated with Eto and IL-4 for 2h. Right panel shows the quantification of PLA signal (n = 4 biological replicates per group). Scale bars 5 μm.

(**I**) PU.1 CUT&Tag binding enrichment of Thio-PMs from *Stat6*$^{WT/-}$, *Stat6*$^{S807A/-}$ and *Stat6*$^{S807E/-}$ mice after IL-4 treatment (n = 3 biological replicates per group), which was assessed by qPCR. B-1/B-2, two PU.1-binding sties around *Brca1* locus. U-1/U-2/U-3, three PU.1-binding sties around *Ube2t* locus.

(**J**) Immunoblots of BRCA1 and UBE2T in Thio-PMs from *Stat6*$^{WT/WT}$, *Stat6*$^{S807A/S807A}$ and *Stat6*$^{S807E/S807E}$ mice with indicated treatments. DB2313, an inhibitor of PU.1.

(**K**) Immunoblots of γH2AX in Thio-PMs from *Stat6*$^{WT/-}$, *Stat6*$^{S807A/-}$ and *Stat6*$^{S807E/-}$ mice with indicated repair period.

The blot data are representative of three biologically independent repeats (G, J and K). Data are mean ± s.e.m. p-value was calculated by one-way ANOVA with Dunnett's correction.

Figure 5: Ser807-phosphorylated STAT6 alleviates macrophage senescence.

(**A**, **B**) mRNA of senescence markers (A) and SASP (B) of Thio-PMs from *Stat6*$^{WT/-}$, *Stat6*$^{S807A/-}$ and *Stat6*$^{S807E/-}$ mice after Eto-induced senescence (*n* = 3 biological replicates per group).

(**C**) EdU staining (EdU, green; DAPI, blue) of Thio-PMs from *Stat6*$^{WT/-}$, *Stat6*$^{S807A/-}$ and *Stat6*$^{S807E/-}$ mice after Eto-induced senescence. Scale bars 50 μm.

(**D**) The quantification of EdU positive cells in (C) (*n* = 3 biological replicates per group).

(**E**) SA-β Gal staining of Thio-PMs from *Stat6*$^{WT/-}$, *Stat6*$^{S807A/-}$ and *Stat6*$^{S807E/-}$ mice after Eto-induced senescence. Arrows indicate the positive cells. Scale bars 100 μm.

(**F**) The quantification of SA-β Gal positive cells in (E) (*n* = 4 biological replicates per group).

(**G**) Lipofuscin staining of Thio-PMs from *Stat6*$^{WT/-}$, *Stat6*$^{S807A/-}$ and *Stat6*$^{S807E/-}$ mice after Eto-induced senescence. Arrows indicate the positive cells. Scale bars 50 μm. Right panel shows the quantification (*n* = 3 biological replicates per group).

(**H**) Diagram of experiments design.

(**I**) Flow cytometry analysis of transferred Res-PMs in peritoneum, which were gated on CD45.2^{+} cells (collected more than 0.8 million per mouse). Right panel shows the quantification (*n* = 5 biological replicates).

(**J**) Bacteria burden in peritoneum of *Stat6*$^{WT/-}$, *Stat6*$^{S807A/-}$ and *Stat6*$^{S807E/-}$ mice 24 h after *E. coli* injection (*n* = 5 biological replicates per group).

(**K**) Burden of senescent MEFs in peritoneum of *Stat6*$^{WT/WT}$, *Stat6*$^{S807A/S807A}$ and *Stat6*$^{S807E/S807E}$ mice 3 days after injection of senescent MEFs (*n* = 6 biological replicates per group).

Data are mean ± s.e.m. p-value was calculated by one-way ANOVA with Dunnett's correction.

Figure 6: Ser807-phosphorylated STAT6 alleviates tissue senescence and improves healthspan in mice.

(**A**–**C**) Motor function tests of *Stat6*$^{WT/WT}$ (*n* = 9), *Stat6*$^{S807A/S807A}$ (*n* = 10) and *Stat6*$^{S807E/S807E}$ (*n* = 10) mice, including rotarod (A), hanging (B), treadmill (C).

(**D**) Y maze test of *Stat6*$^{WT/WT}$ (*n* = 9), *Stat6*$^{S807A/S807A}$ (*n* = 10) and *Stat6*$^{S807E/S807E}$ (*n* = 10) mice.

(**E**) Bone density of *Stat6*$^{WT/WT}$ (*n* = 9), *Stat6*$^{S807A/S807A}$ (*n* = 10) and *Stat6*$^{S807E/S807E}$ (*n* = 10) mice.

(**F**) mRNA expression of senescence markers in eWAT, liver and lung from *Stat6*$^{WT/WT}$, *Stat6*$^{S807A/S807A}$ and *Stat6*$^{S807E/S807E}$ mice (*n* = 7 per group).

(**G**) mRNA expression of SASP in eWAT, liver and lung from *Stat6*$^{WT/WT}$, *Stat6*$^{S807A/S807A}$ and *Stat6*$^{S807E/S807E}$ mice (*n* = 7 per group). The statistical p-value are shown in Supplementary Fig. 6A.

(**H**) SA-β Gal staining of eWAT from *Stat6*$^{WT/WT}$, *Stat6*$^{S807A/S807A}$ and *Stat6*$^{S807E/S807E}$ (*n* = 3 biological replicates per group). The right panel shows the quantification.

(**I**) Experiment design for transfer of BMDMs to aged mice.

(**J**) Body wight loss of aged mice after BMDMs transfer (*n* = 6 in PBS group, *n* = 7 in transfer groups).

(**K**–**N**) Physical analysis of aged mice after BMDMs transfer (*n* = 6 in PBS group, *n* = 7 in transfer groups), containing rotarod test (K), hanging test (L), treadmill test (M) and Y maze test (N).

(**O**, **P**) mRNA expression of senescence markers (O) and SASP (P) in tissues (eWAT, liver and spleen) from aged mice after BMDMs transfer (*n* = 6 in PBS group, *n* = 7 in transfer groups).

(**Q**) SA-β Gal staining of eWAT from aged mice after BMDMs transfer (*n* = 4 per group). Right panel shows the quantification.

Mice in (A–H) were 9-month-old. Data are mean ± s.e.m. p-value was calculated by one-way ANOVA with Dunnett's correction.

Figure 7: Ser807 non-phosphorylated *Stat6*$^{S807A/S807A}$ knock-in mice are sensitive to bleomycin-induced pulmonary fibrosis.

(**A**) mRNA expression of *Brca1* and *Ube2t* in *Stat6*$^{WT/WT}$, *Stat6*$^{S807A/S807A}$ and *Stat6*$^{S807E/S807E}$ alveolar macrophages (AM) with indicated treatment. The freshly isolated AMs were treated with IL-4 (10 ng/mL) and DB1213 (10 nM) for 16 h (n = 3 biological replicates per group).

(**B**) Design of bleomycin-induced pulmonary fibrosis model.

(**C**) mRNA expression of *p16-Ink4a* and *p21-Cip1* in AMs isolated from *Stat6*$^{WT/WT}$, *Stat6*$^{S807A/S807A}$ and *Stat6*$^{S807E/S807E}$ mice 7 days after bleomycin treatment (n = 3 biological replicates per group).

(**D**) SA-β Gal staining of alveolar macrophages isolated from *Stat6*$^{WT/WT}$, *Stat6*$^{S807A/S807A}$ and *Stat6*$^{S807E/S807E}$ mice 7 days after bleomycin treatment. Right panel shows the quantification (n = 3 biological replicates per group). Arrows indicate positive cells. Scale bars 25 μm.

(**E**) Representative images of H&E, Masson' trichrome and Sirius red staining of lung sections from *Stat6*$^{WT/WT}$, *Stat6*$^{S807A/S807A}$ and *Stat6*$^{S807E/S807E}$ mice 20 days after bleomycin treatment. Scale bars 200 μm.

(**F**) Fibrosis scores of *Stat6*$^{WT/WT}$, *Stat6*$^{S807A/S807A}$ and *Stat6*$^{S807E/S807E}$ mice under bleomycin-induced pulmonary fibrosis (n = 18 biological replicates per group).

(**G**) Survival curves of *Stat6*$^{WT/WT}$, *Stat6*$^{S807A/S807A}$ and *Stat6*$^{S807E/S807E}$ mice with bleomycin-induced pulmonary fibrosis (n = 11 biological replicates per group).

(**H**) Immunoblots of COL1A1, α-SMA, pSMAD2/3 and P16-INK4A in lung from *Stat6*$^{WT/WT}$, *Stat6*$^{S807A/S807A}$ and *Stat6*$^{S807E/S807E}$ mice 20 days after bleomycin treatment, representative of at least five biologically replicates.

(**I**) Design of AMs transfer in a bleomycin-induced pulmonary fibrosis model in (J–L).

(**J**) mRNA expression of senescence and fibrosis markers in lungs of mice treated with AMs (n = 5 biological replicates per group) or PBS control (n = 4 biological replicates).

(**K**) Representative Masson's trichrome-stained images of lung sections from mice treated with AMs or PBS control. Scale bars 200 μm.

(**L**) Fibrosis scores in mice treated with AMs or PBS control (n = 5 biological replicates per group).

Data are mean ± s.e.m. One-way ANOVA with Dunnett's correction (A, C, D, F, J and L), Mantel-Cox's log-rank test (G).

Figure 8: STAT6 phosphorylation at Ser817 is associated with COPD in humans.

(**A**) Immunoblots of pSTAT6 (pS817) and γH2AX in hMDMs under indicated treatment.

(**B**) Quantification of pSTAT6 (pS817)/α-Tubulin in (A) (*n* = 5 biological replicates per group).

(**C**) mRNA expression of *BRCA1* and *UBE2T* in hMDMs expressing hSTAT6 mutants (WT, S817A, S817E) after 16-h hIL-4 treatment (*n* = 5 biological replicates per group).

(**D**) DNA repair capacity of THP-1-differentiated macrophages expressing hSTAT6 mutants (WT, S817A, S817E). Right panel shows the quantification (*n* = 3 independent experiments).

(**E**) mRNA expression of *P16-INK4A* and *P21-CIP1* in THP-1-differentiated macrophages expressing hSTAT6 mutants (WT, S817A, S817E) under Eto-induced senescence (*n* = 3 biological replicates per group).

(**F**) Phagocytosis assay of THP-1-differentiated macrophages expressing hSTAT6 mutants (WT, S817A, S817E). All groups had 30-min phagocytosis period. Right panel shows the quantification (*n* = 4 biological replicates per group).

(**G**) Representative image of lung sections from control and COPD donors. Scale bar 100 μm.

(**H**) Quantification of $P16^+$ cells in lungs from control and COPD donors (*n* = 6 biological replicates per group).

(**I**) Quantification of $P16^+$ macrophages ($CD68^+$) in lungs from control and COPD donors (*n* = 6 biological replicates per group).

(**J**) Immunoblots of pSTAT6 (pS817), P16-INK4A and γH2AX in lungs from control, smoker, and COPD donors (*n* = 4 biological replicates per group).

(**K**) Quantification of pSTAT6 (pS817)/tSTAT6 in lungs from control, smoker, and COPD donors (*n* = 4 biological replicates per group).

(**L**) Spearman's correlation between pSTAT6 (pS817)/tSTAT6 and γH2AX in human lungs from control (*n* = 10), smoker (*n* = 4), and COPD donors (*n* = 10).

(**M**) Spearman's correlation between pSTAT6 (pS817)/tSTAT6 and P16-INK4A in human lungs from control (*n* = 10), smoker (*n* = 4), and COPD donors (*n* = 10).

Data are mean ± s.e.m. p-value was calculated by paired two-tailed Student's t test (B, C and D) one-way ANOVA with Dunnett's correction (E, F and K), unpaired two-tailed Student's t test (H and I), two-tailed Spearman's correlation coefficient analysis (L and M).

Editorial Summary

STAT6 mitigates cellular aging and senescence by regulating the expression of DNA repair genes. However, the upstream signals driving the activation of this non-canonical STAT6 function have not been identified. Here, the authors identify DNA-PK as a key kinase mediating STAT6 phosphorylation in murine and human macrophages and show that this post-translational modification is required to prevent macrophage senescence and protects animals from senescence-driven lung fibrosis and aging.

Peer Review Information: ***Nature Communications*** **thanks Christina Camell, Conor Finlay and Bruno Guigas for their contribution to the peer review of this work. A peer review file is available.**

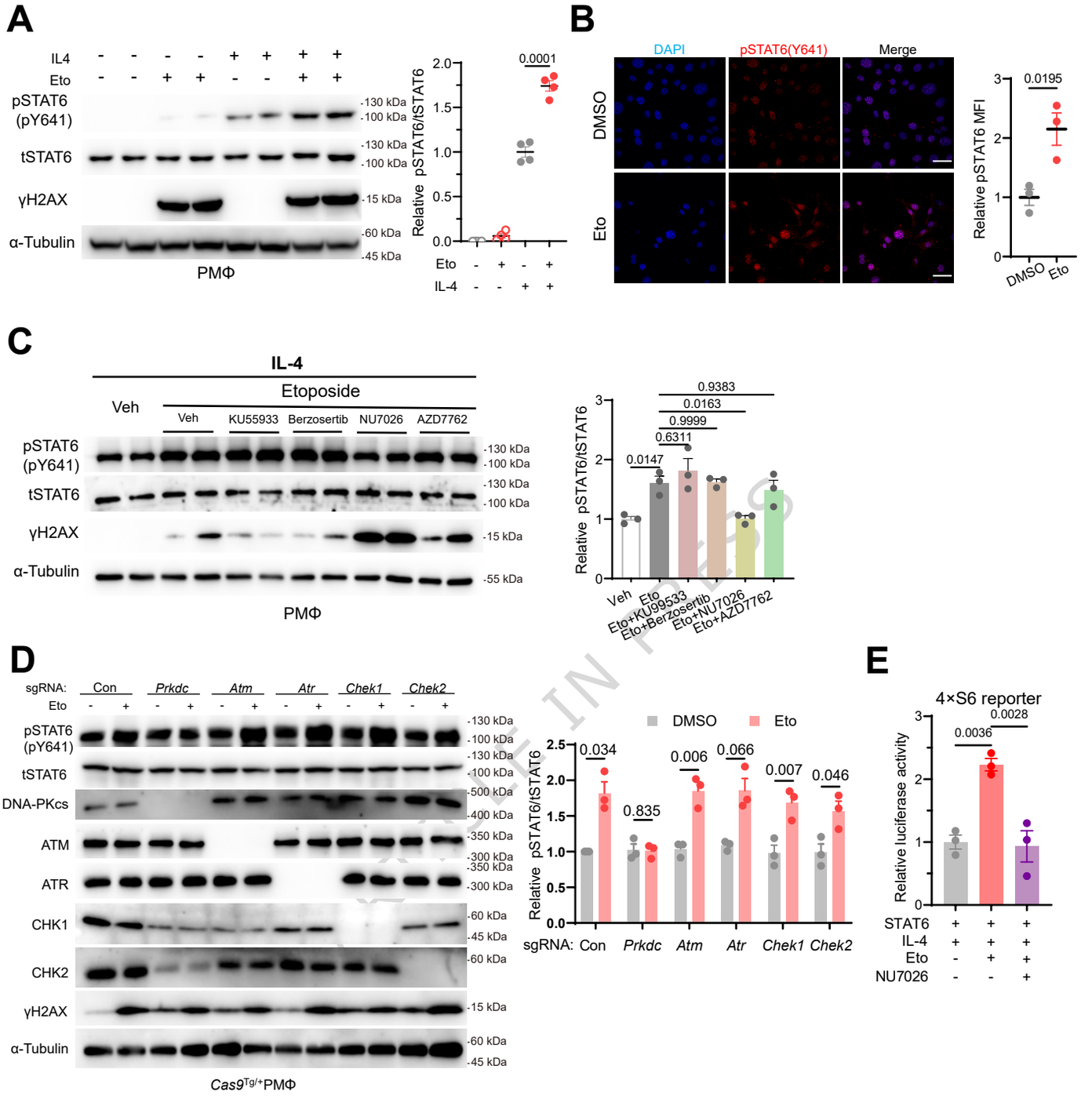
A
IL4
Eto
pSTAT6 (pY641)
tSTAT6
γH2AX
α-Tubulin
130 kDa
100 kDa
15 kDa
60 kDa
45 kDa
PMΦ
Relative pSTAT6/tSTAT6
0.0001
B
DAPI
pSTAT6(Y641)
Merge
DMSO
Eto
Relative pSTAT6 MFI
0.0195
C
IL-4
Etoposide
Veh
KU55933
Berzosertib
NU7026
AZD7762
55 kDa
0.9383
0.0163
0.9999
0.6311
0.0147
Eto+KU99533
Eto+Berzosertib
Eto+NU7026
Eto+AZD7762
D
sgRNA:
Con
Prkdc
Atm
Atr
Chek1
Chek2
DNA-PKcs
ATM
ATR
CHK1
CHK2
500 kDa
400 kDa
350 kDa
300 kDa
Cas9Tg/+PMΦ
0.034
0.835
0.006
0.066
0.007
0.046
E
4×S6 reporter
Relative luciferase activity
0.0028
0.0036
STAT6
IL-4
Eto
NU7026

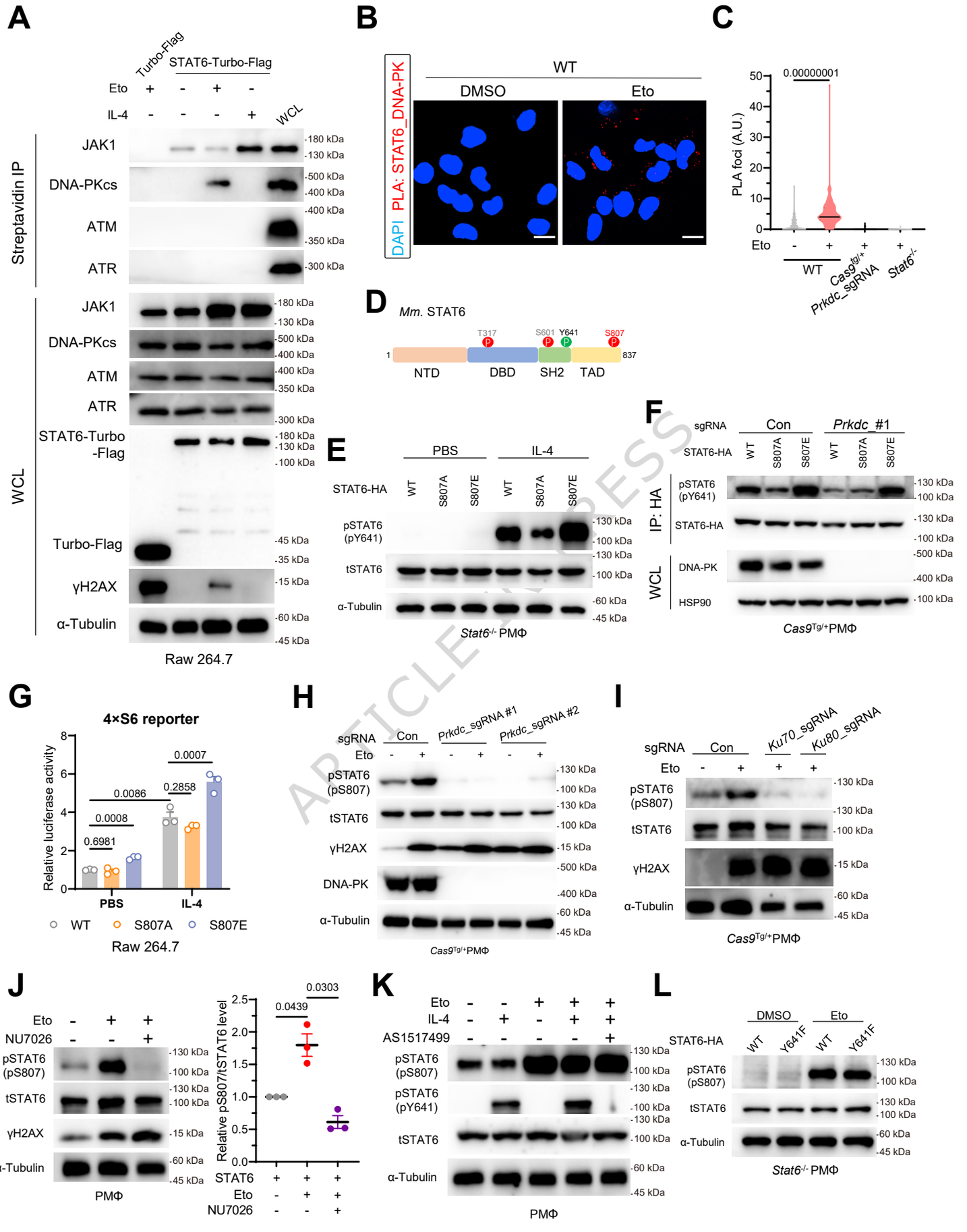
A
Turbo-Flag
STAT6-Turbo-Flag
Eto + - + -
IL-4 - - - +
WCL
Streptavidin IP
JAK1
DNA-PKcs
ATM
ATR
WCL
JAK1
DNA-PKcs
ATM
ATR
STAT6-Turbo-Flag
Turbo-Flag
γH2AX
α-Tubulin
Raw 264.7
B
WT
DMSO
Eto
DAPI PLA: STAT6_DNA-PK
C
PLA foci (A.U.)
0.00000001
Eto - + + +
WT
Cas9tg/+ Prkdc_sgRNA
Stat6-/-
D
Mm. STAT6
T317 S601 Y641 S807
1 837
NTD DBD SH2 TAD
E
PBS IL-4
STAT6-HA WT S807A S807E WT S807A S807E
pSTAT6 (pY641)
tSTAT6
α-Tubulin
Stat6-/- PMΦ
F
sgRNA Con Prkdc_#1
STAT6-HA WT S807A S807E WT S807A S807E
IP: HA
pSTAT6 (pY641)
STAT6-HA
WCL
DNA-PK
HSP90
Cas9Tg/+PMΦ
G
4×S6 reporter
Relative luciferase activity
0.6981
0.0008
0.0086
0.2858
0.0007
PBS IL-4
WT S807A S807E
Raw 264.7
H
sgRNA Con Prkdc_sgRNA #1 Prkdc_sgRNA #2
Eto - + - + - +
pSTAT6 (pS807)
tSTAT6
γH2AX
DNA-PK
α-Tubulin
Cas9Tg/+PMΦ
I
sgRNA Con Ku70_sgRNA Ku80_sgRNA
Eto - + + +
pSTAT6 (pS807)
tSTAT6
γH2AX
α-Tubulin
Cas9Tg/+PMΦ
J
Eto - + +
NU7026 - - +
pSTAT6 (pS807)
tSTAT6
γH2AX
α-Tubulin
PMΦ
Relative pS807/tSTAT6 level
0.0439
0.0303
STAT6 + + +
Eto - + +
NU7026 - - +
K
Eto - - + + +
IL-4 - + - + +
AS1517499 - - - - +
pSTAT6 (pS807)
pSTAT6 (pY641)
tSTAT6
α-Tubulin
PMΦ
L
DMSO Eto
STAT6-HA WT Y641F WT Y641F
pSTAT6 (pS807)
tSTAT6
α-Tubulin
Stat6-/- PMΦ

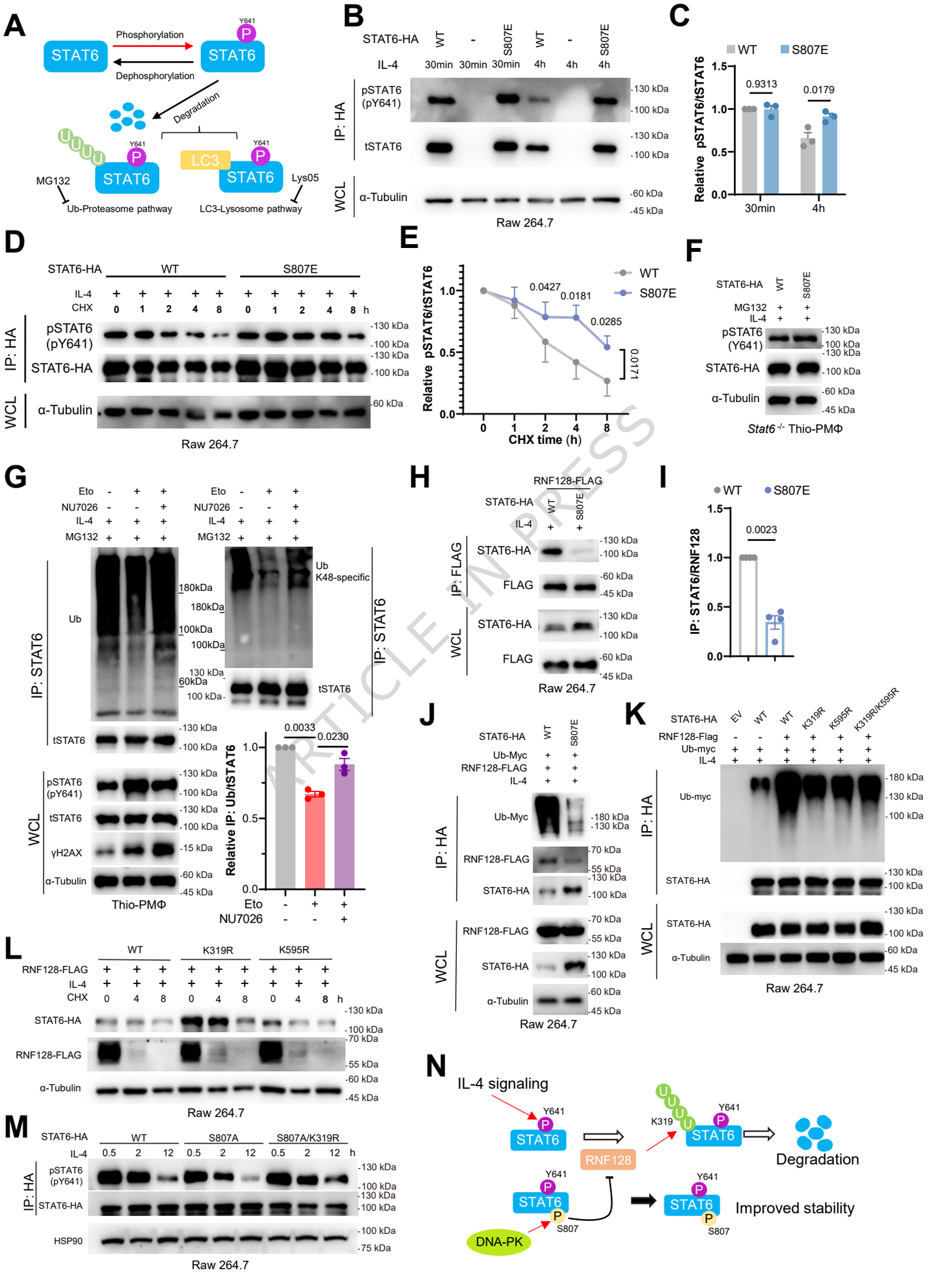

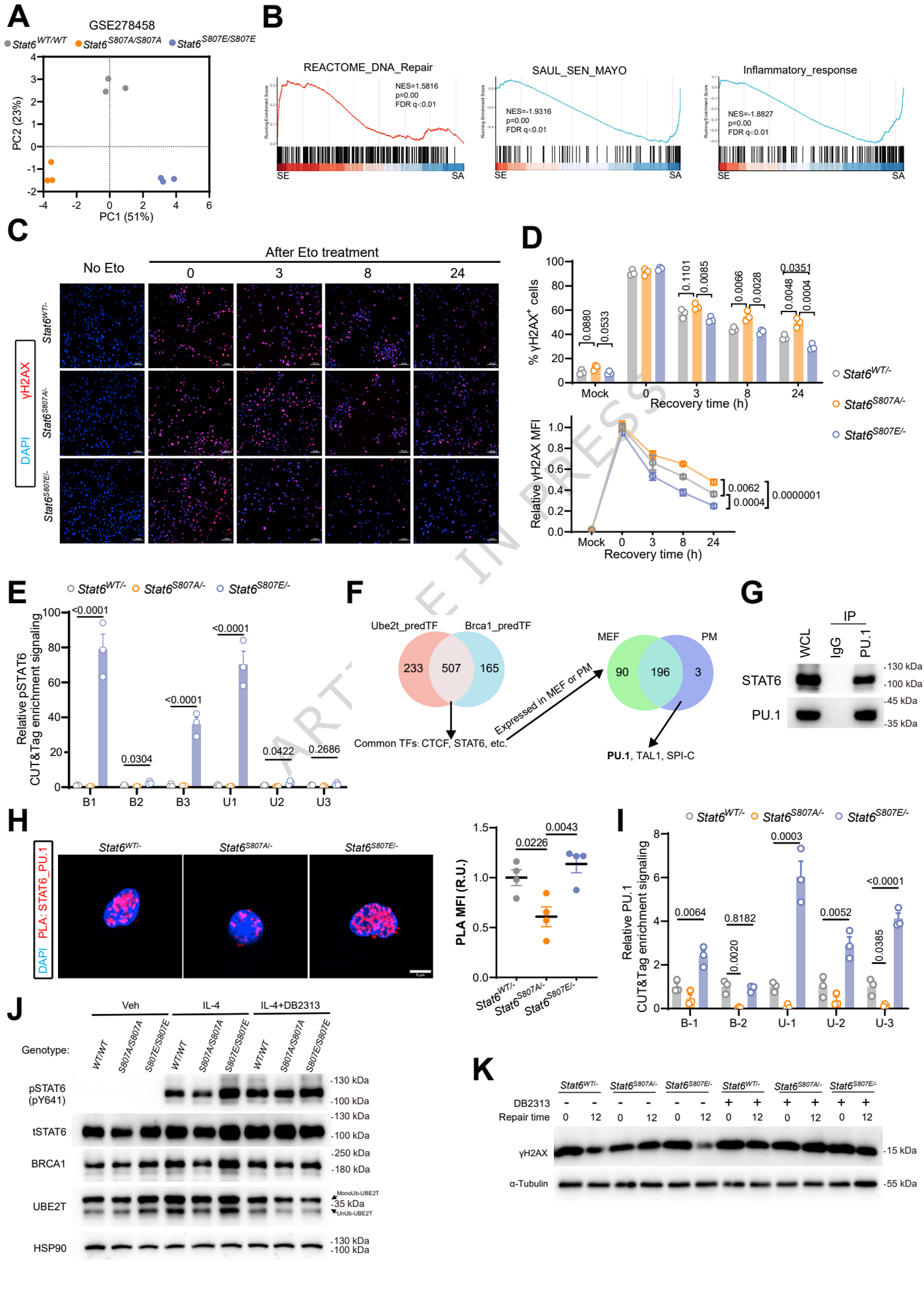
A
GSE278458
Stat6WT/WT
Stat6S807A/S807A
Stat6S807E/S807E
PC2 (23%)
PC1 (51%)
B
REACTOME_DNA_Repair
NES=1.5816
p=0.00
FDR q<0.01
SAUL_SEN_MAYO
NES=-1.9316
p=0.00
FDR q<0.01
Inflammatory_response
NES=-1.8827
p=0.00
FDR q<0.01
SE
SA
C
No Eto
After Eto treatment
0
3
8
24
Stat6WT/-
Stat6S807A/-
Stat6S807E/-
DAPI
γH2AX
D
% γH2AX+ cells
0.0880
0.0533
0.1101
0.0085
0.0066
0.0028
0.0351
0.0048
0.0004
Mock
Recovery time (h)
Relative γH2AX MFI
0.0062
0.0004
0.0000001
E
Relative pSTAT6 CUT&Tag enrichment signaling
<0.0001
0.0304
<0.0001
<0.0001
0.0422
0.2686
B1
B2
B3
U1
U2
U3
F
Ube2t_predTF
Brca1_predTF
233
507
165
Common TFs: CTCF, STAT6, etc.
Expressed in MEF or PM
MEF
PM
90
196
3
PU.1, TAL1, SPI-C
G
IP
WCL
IgG
PU.1
STAT6
PU.1
130 kDa
100 kDa
45 kDa
35 kDa
H
DAPI
PLA: STAT6_PU.1
PLA MFI (R.U.)
0.0226
0.0043
I
Relative PU.1 CUT&Tag enrichment signaling
0.0064
0.8182
0.0020
0.0003
0.0052
0.0385
<0.0001
B-1
B-2
U-1
U-2
U-3
J
Veh
IL-4
IL-4+DB2313
Genotype:
WT/WT
S807A/S807A
S807E/S807E
pSTAT6 (pY641)
tSTAT6
BRCA1
UBE2T
MonoUb-UBE2T
UnUb-UBE2T
HSP90
130 kDa
100 kDa
250 kDa
180 kDa
35 kDa
K
DB2313
Repair time
γH2AX
α-Tubulin
15 kDa
55 kDa

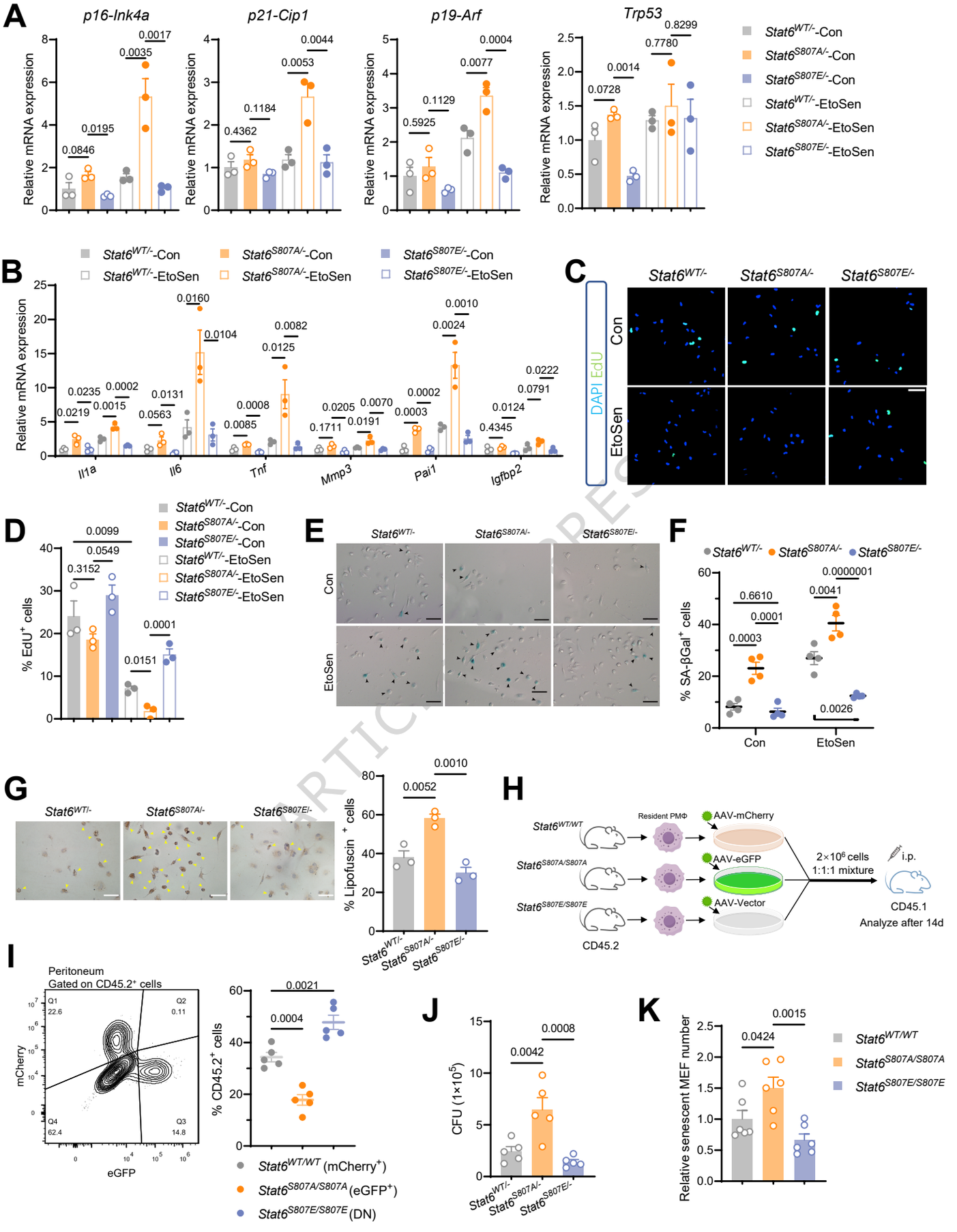
A
p16-Ink4a
p21-Cip1
p19-Arf
Trp53
Relative mRNA expression
Stat6WT/--Con
Stat6S807A/--Con
Stat6S807E/--Con
Stat6WT/--EtoSen
Stat6S807A/--EtoSen
Stat6S807E/--EtoSen
B
Il1a
Il6
Tnf
Mmp3
Pai1
Igfbp2
C
DAPI EdU
Con
EtoSen
D
% EdU+ cells
E
F
% SA-βGal+ cells
G
% Lipofuscin+ cells
H
Resident PMΦ
AAV-mCherry
AAV-eGFP
AAV-Vector
2×10⁶ cells
1:1:1 mixture
i.p.
CD45.1
Analyze after 14d
CD45.2
I
Peritoneum
Gated on CD45.2+ cells
mCherry
eGFP
% CD45.2+ cells
Stat6WT/WT (mCherry+)
Stat6S807A/S807A (eGFP+)
Stat6S807E/S807E (DN)
J
CFU (1×10⁵)
K
Relative senescent MEF number

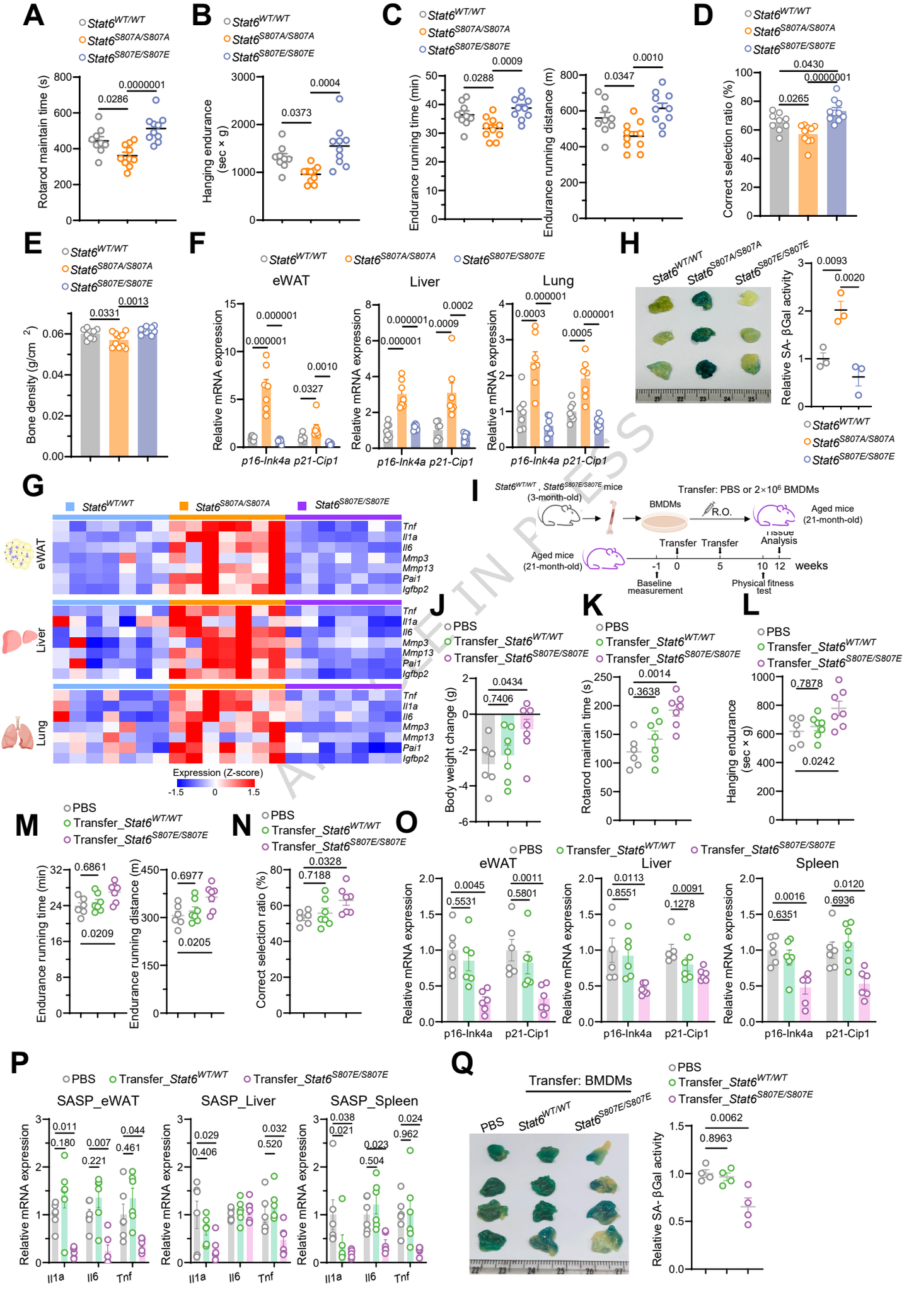
A
B
C
D
E
F
G
H
I
J
K
L
M
N
O
P
Q
Stat6WT/WT
Stat6S807A/S807A
Stat6S807E/S807E
Rotarod maintain time (s)
Hanging endurance (sec × g)
Endurance running time (min)
Endurance running distance (m)
Correct selection ratio (%)
Bone density (g/cm 2)
eWAT
Liver
Lung
Relative mRNA expression
p16-Ink4a
p21-Cip1
Relative SA- βGal activity
Tnf
Il1a
Il6
Mmp3
Mmp13
Pai1
Igfbp2
Expression (Z-score)
Stat6WT/WT , Stat6S807E/S807E mice
(3-month-old)
BMDMs
R.O.
Aged mice
(21-month-old)
Transfer: PBS or 2×10⁶ BMDMs
Transfer
Tissue Analysis
weeks
Baseline measurement
Physical fitness test
PBS
Transfer_Stat6WT/WT
Transfer_Stat6S807E/S807E
Body weight change (g)
Spleen
SASP_eWAT
SASP_Liver
SASP_Spleen
Transfer: BMDMs